Naval Research Laboratory

Washington, DC 20375-5320

NRL/MR/6707--00-8430

Theoretical Overview of the Large Area Plasma Processing System (LAPPS)

WALLACE MANHEIMER

Senior Scientist Fundamental Plasma Processes
Plasma Physics Division

RICHARD FERNSLER

Charged Particle Physics Branch
Plasma Physics Division

MARTIN LAMPE

Senior Scientist Intense Particle Beams and Plasma Processing
Plasma Physics Division

ROBERT MEGER

Charged Particle Physics Branch
Plasma Physics Division

April 17, 2000

REPORT DOCUMENTATION PAGE

Form Approved
OMB No. 0704-0188

1. AGENCY USE ONLY (*Leave Blank*)	2. REPORT DATE	3. REPORT TYPE AND DATES COVERED
	April 17, 2000	Interim

4. TITLE AND SUBTITLE

Theoretical Overview of the Large Area Plasma Processing System (LAPPS)

5. FUNDING NUMBERS

6. AUTHOR(S)

Wallace M. Manheimer, Richard Fernsler, Martin Lampe, and Robert Meger

7. PERFORMING ORGANIZATION NAME(S) AND ADDRESS(ES)

Naval Research Laboratory
Washington, DC 20375-5320

8. PERFORMING ORGANIZATION REPORT NUMBER

NRL/MR/6707--00-8430

9. SPONSORING/MONITORING AGENCY NAME(S) AND ADDRESS(ES)

Office of Naval Research
800 N. Quincy Street
Arlington, VA 22217

10. SPONSORING/MONITORING AGENCY REPORT NUMBER

11. SUPPLEMENTARY NOTES

12a. DISTRIBUTION/AVAILABILITY STATEMENT

Approved for public release; distribution unlimited.

12b. DISTRIBUTION CODE

13. ABSTRACT (*Maximum 200 words*)

A large area plasma processing system (LAPPS) is under development at NRL. In LAPPS, the plasma is generated by a sheet electron beam with voltages and current densities of the order of kilovolts and tens of milliamps per cm^2. The plasma dimensions are a meter square by a few centimeters thick. The beam is guided by a magnetic field of 50-300 Gauss. Since an electron beam of this type efficiently ionizes any gas, high electron densities, $n \sim 10^{12} - 10^{13}$ cm^{-3} are easily are easily generated at 30-100 mtorr background pressure. In addition to large area and high electron density, LAPPS has advantages for plasma processing. These include independent control of ion and free radical fluxes to the surface, very high uniformity, very low electron temperature ($Te < 1eV$, but can be controllably increased to a desired value) and a geometry that is well suited for many applications. This paper sketches an initial theoretical overview of issues in LAPPS and compares aspects of the theory to a preliminary experiment.

14. SUBJECT TERMS

15. NUMBER OF PAGES
47

16. PRICE CODE

17. SECURITY CLASSIFICATION OF REPORT	18. SECURITY CLASSIFICATION OF THIS PAGE	19. SECURITY CLASSIFICATION OF ABSTRACT	20. LIMITATION OF ABSTRACT
UNCLASSIFIED	UNCLASSIFIED	UNCLASSIFIED	UL

NSN 7540-01-280-5500

Standard Form 298 (Rev. 2-89)
Prescribed by ANSI Std 239-18
298-102

1. Introduction

As the technology of plasma processing progresses, there is a continuing demand for higher plasma density, uniformity over large areas, and greater control over plasma parameters to optimize the processes of etching, deposition and surface treatment. A number of new high density plasma sources are in use, notably electron cyclotron resonance [1,2], inductively coupled plasma [3,4], and helicon reactors [5,6]. All of these technologies, as well as the older commercial technology of capacitively-coupled rf discharges, couple energy electromagnetically from the external power source into heating of the plasma electrons, which then collisionally ionize the gas. At the Naval Research Laboratory we are developing a different type of plasma reactor called LAPPS (for large-area plasma processing system), in which a magnetically guided sheet electron beam is used to ionize the gas. The LAPPS device is shown schematically in Fig. 1. We have routinely produced large-area uniform plasma sheets with density in excess of 10^{12} cm^{-3}. In the present design, the plasma will occupy a volume roughly one meter square by a few cm thick. This technology is quite versatile, with potential applications in a number of areas including etching, deposition and surface treatment, and it offers many advantages. Foremost among these is the independent control that can be exercised over each of the important processing parameters: the plasma density, the spatial volume in which ionization occurs, the electron temperature (which strongly influences the chemistry), the flux of ions to the workpiece, the ion bombardment energy, and the flux of free radicals to the workpiece. For additional control over chemistry and substrate charging, the beam can easily be operated in either a pulsed or cw mode. Furthermore, electron beams are unusually efficient plasma sources, with roughly half the deposited energy going into ionization, and only a small fraction going into low-lying excitations.

LAPPS grew out of the NRL agile mirror project, where the goal was to produce a sheet plasma that could be reoriented electronically to steer a radar beam [7–13], or to serve as a fast, high-power microwave switch [14]. As a result of this work, which was carried out over a period of seven years, considerable understanding was gained of plasma production by sheet electron beams [10,11], and beam production by hollow cathodes [14]. It is this knowledge base that is now being applied to LAPPS. Typical operating parameters in LAPPS are gas pressure 10 to 500 mTorr, beam voltage several keV, beam current density 5-50 mA/cm^2, and plasma density up to 5×10^{12} cm^{-3}. A magnetic field of 50–300 G is used to confine the beam and thereby produce a planar plasma. In experiments done to date, the beam source has been the hollow cathode source used in the agile mirror. Hollow cathodes offer advantages over both thermionic electron sources (which rarely are consistent with the corrosive gases at relative high pressure in processing systems), and thin foils to separate beam production from plasma (which greatly degrade the beam energy). We are now investigating improved hollow cathode sources which may offer steady state operation at greater efficiency [15,16].

Several initial LAPPS experiments have been done. These include a demonstration of plasma sheet production with high uniformity over areas up to 60 cm × 60 cm, approximate determination of the ion flux to an adjacent substrate, and etching of a patterned photo-resist. The latter two experiments were done in oxygen, but the LAPPS scheme works well in any gas, and over a wide pressure range. Shown in Fig. 2 are the photoresist etch patterns, which were

Manuscript approved February 8, 2000.

achieved at an etch rate exceeding 6 μm per minute of beam on-time. In this initial experiment the etching was done without rf bias, and the undercut seen in Fig. 2 indicates that the etch was nearly isotropic, as expected. Etch experiments with rf bias are in progress. Initial results indicate a highly anisotropic etch [17].

In this paper we present an initial analysis of LAPPS, including a brief discussion of the preliminary experiments. (Full details of the experiments will be reported separately.) LAPPS differs from most of the traditional plasma sources in many ways, most notably in that the plasma is created by an externally controllable beam rather than by dissipating electromagnetic energy in the plasma, and ions are transported to the workpiece across a magnetic field, whose magnitude is such that the electrons are strongly magnetized but the ions are essentially unmagnetized. In the next two sections, we consider the production of plasma and free radicals by electrons beams in gas, and for specificity we apply the analysis to oxygen. In Sec. 4 we discuss cross-field ion transport to a substrate. We show first that for cross field flow, the usual Bohm condition holds between the plasma and sheath. Furthermore, in the parameter regime of interest to LAPPS the magnetic field has little effect on the sheath, although for very high fields it would reduce the dc sheath potential. We then show that the flux depends on the value of magnetic field, the pressure, the distance from the plasma source to the substrate, the question of whether the substrate is a conductor or insulator, and (in the latter case) the dc bias of the substrate. We also consider the issue of flux uniformity, and show that a very high degree of uniformity is to be expected over a large area insulating substrate. These results are compared to a preliminary experiment in Sec. 5. Finally in Sec. 6 we summarize and briefly discuss new experiments underway.

2. Beam Propagation and Plasma Production

In this section we discuss the production and maintenance of a plasma by a magnetized electron beam. The key collisional processes considered are energy loss, ionization, and elastic scattering. The energy loss rate, in cgs units, for a non-relativistic beam in gas is given by the Bethe formula [18],

$$\frac{d\varepsilon}{ds} = \frac{2\pi n_{mol} Z_{mol} e^4}{\varepsilon} \ln\frac{\varepsilon}{\varepsilon_0}, \tag{1}$$

where ε is the beam energy, s is the distance traversed by a beam electron, n_{mol} is the number density of neutral gas molecules, Z_{mol} is the number of bound electrons in a molecule, e is the electron charge, and $\varepsilon_0 \sim 100$ eV is the mean excitation energy of the gas molecules. Integration of Eq. (1) indicates that the range of the beam electrons is approximately equal to

$$R = \frac{\varepsilon^2}{4\pi n_{mol} Z_{mol} e^4}\left(\ln\frac{\varepsilon}{\varepsilon_0}\right)^{-1}. \tag{2}$$

The range R must exceed the system length L in order to maintain uniformity. In the case of oxygen, Eqs. (1) and (2) indicate that the requirement is

$$n_{mol} L < 2.4\times10^{11}\frac{V^2}{\ln(V/100)}. \tag{3}$$

where V is now the beam energy in eV. As an example, if L = 100 cm and V = 3 keV, the molecule density should be $n_{mol} \le 5.4\times10^{15}$ cm^{-3}, i.e. pressure $\le$ 150 mTorr at room temperature.

The volumetric ionization rate, i.e. the rate of increase of plasma electron density n_e due to beam ionization, is

$$S = (1+g)\frac{J_b}{e}\frac{1}{\bar{\varepsilon}_i}\frac{d\varepsilon}{ds} \equiv (1+g)\frac{J_b}{e} n_{mol}\sigma_i \tag{4}$$

where J_b is the beam current density flowing in the z direction and $\bar{\varepsilon}_i$ is the mean energy deposited per electron-ion pair created. Here $g \equiv v_\perp^{(rms)}/v_z$ is a correction factor representing the angular spread of electron velocities within the beam; in propagating an axial distance Δz, a beam electron traverses on average a path length $\Delta s = (1+g)\Delta z$. The quantity $\sigma_i \equiv (d\varepsilon/ds)(n_{mol}\bar{\varepsilon}_i)^{-1}$ is an effective ionization cross section, which includes the ionization produced by energetic secondaries, tertiaries, etc. In oxygen[19] $\bar{\varepsilon}_i \cong 31$ eV, and consequently

$$\sigma_i = \frac{1.3\times10^{-13}}{V}\ln(V/100)\,cm^2, \tag{5}$$

where V is in eV. Note that as the beam propagates in z, the beam energy V decreases and thus σ_i increases. It should also be noted that $\bar{\varepsilon}_i \cong 31$ eV (a number which is typical for all gas species) is very low compared to the energy input per electron ion pair for ICP, helicon or ECR discharges. Thus LAPPS can be significantly more efficient than typical processing discharges even if L << R and only a fraction of the beam energy is deposited in the plasma.

Elastic scattering of beam electrons off gas atoms increases the angular spread of beam velocities, at a rate

$$\frac{dg^2}{dz} = 2n_{mol}\sigma_m, \tag{6a}$$

where [20]

$$\sigma_m(\varepsilon) = \frac{\pi Z_{mol}{}^2 e^4}{2\alpha\varepsilon^2}\ln(V/V_1) \tag{6b}$$

is the momentum-loss cross-section for beam-molecule collisions. Here α is the number of atoms per molecule, and $V_1 = 1.7[Z_{mol}/\alpha]^{2/3}$. In the absence of any confining force, scattering would lead to spatial spreading of the beam. Therefore a longitudinal magnetic field B is applied to confine the beam. As shown in [11], a strong field limits the increase in the mean-squared beam thickness to less than $2r_{max}{}^2$ over the beam range R, where $r_{max} \cong 3.1V^{1/2}/B$ is the maximum electron gyroradius radius in cm and B is in G. A 200 G field is therefore sufficient to keep the beam thickness approximately constant if the initial thickness is a few cm and $V \leq 3$ keV. In the operating regime for LAPPS, the beam energy loss rate from Eq. (1) is generally more rapid than the elastic scattering rate from Eq. (6), and one can assume $g < 1$.

The efficiency of the beam in ionizing gas increases with propagation distance z, because of the increase of σ_i as the beam energy decreases, and also because of the increase of the geometric factor g due to elastic scattering. As a result, the plasma density will tend to increase with z. For applications requiring a high degree of uniformity in the z direction, the system length L should be limited to L << R. In this case, it is advantageous to collect and recover the unused beam energy. In addition, there are several adjustments which can easily be made to minimize any residual process non-uniformity: the magnetic field can be tapered, and/or the processing stage can be tilted with respect to the plasma sheet. In addition, the substrate could be rotated during processing, or in some cases moved through the LAPPS device on a continuous feed belt.

In LAPPS, the plasma electron temperature T_e will generally be low. The reason is that inelastic (e.g. vibrational) collisions cool the electrons very effectively in molecular gases, and

there are no electric fields to heat them [11]. Langmuir probe measurements on oxygen LAPPS plasmas [21], have given preliminary estimates of the electron temperature of about 0.6 eV. As a consequence, the density of negative ions will be low in an oxygen plasma; the two body dissociative attachment process which creates this ion requires an electron of energy 4 to 8 eV [22]. (For a halogen gases like chlorine, the two body dissociative attachment is exothermic, and negative ions could play a much more important role on cross field ion transport. We will consider this in a future work.)

For simplicity, we shall assume throughout the paper that the dominant ion is O_2^+, with density $n_i = n_e$ in the quasi-neutral bulk plasma. Dissociative recombination between the plasma electrons and positive molecular ions limits the ion density. The volumetric loss rate is βn_e^2, where β is the dissociative recombination rate coefficient. In steady state, if there is no diffusion, the loss rate balances the production rate, and hence

$$n_e = \sqrt{\frac{J_b n_{mol} \sigma_i}{e\beta}}, \tag{6}$$

where we have let g = 1 for simplicity. If diffusion is included, Eq. (6) gives an upper limit for the ion density. For an oxygen plasma in LAPPS [23],

$$\beta(cm^3/s) \sim 2.4 \times 10^{-8} T_e^{-1/2}(eV) \tag{7}$$

while $\sigma_i \sim 10^{-16}$ cm^2 for V = 3×10^3 eV. A beam current density of $J_b \cong 10$ mA/cm^2 is then needed to produce a plasma of density $n_e = 10^{12}$ cm^{-3} in 100 mTorr of oxygen ($n_{mol} \cong 3\times10^{15}$ cm^{-3}). The nominal beam range in that case is R $\cong$ 150 cm.

3. Free-Radical Production

Free radicals which are active in surface processing can be produced directly by beam-impact dissociation (e.g., $e + O_2 \rightarrow e + O + O$, with cross-section σ_d), or beam-impact dissociative ionization (e.g., $e + O_2 \rightarrow 2e + O + O^+$, with cross-section σ_{di}). In addition, radicals can be produced indirectly by beam-impact ionization, with cross-section σ_i, followed by dissociative recombination between a plasma electron and a molecular ion (e.g., $e + O_2^+ \rightarrow O + O$). Dissociation of neutral molecules by plasma-electron impact is usually negligible in beam-produced plasmas, because the electron temperature is too low, $T_e < 1$ eV. The total volumetric production rate of free radicals is thus at most equal to

$$S_r^{max} = \frac{2J_b}{e} n_{mol}(\sigma_i + \sigma_{di} + \sigma_d), \tag{8}$$

under conditions such that every O_2^+ ion undergoes dissociative recombination in the plasma to form two O radicals, and every O^+ ion recombines on a surface to form one O atom. In steady state, the flux of free radicals to a substrate located on one side of the plasma sheet is thus limited to

$$F_r = aS_r^{max} = \frac{2aJ_b n_{mol}(\sigma_i + \sigma_{di} + \sigma_d)}{e} \tag{9}$$

where a is the beam half-thickness. In most cases, σ_i is the largest of the beam-impact cross-sections, but in many molecular gases σ_d is of the order of $\frac{1}{2}\sigma_i$; the cross-section σ_{di} is usually smaller. In oxygen, however, $\sigma_d << \sigma_i$ and beam-impact dissociation can be neglected [24]. Thus dissociative recombination is the dominant process leading to creation of free radicals. For a = 1 cm, and the parameters listed earlier (J_b = 10 mA/cm^2, $n_{mol} = 3\times10^{15}$ cm^{-3} and $\sigma_i = 10^{-16}$ cm^2), the maximum flux of free radicals is about 4×10^{16} atoms/cm^2-s.

In many situations, it is desirable to maximize the flux of ions to the substrate. In those cases, it is generally possible in LAPPS (as discussed in detail in the next section) to choose parameters (plasma density n_e, plasma sheet thickness 2a, standoff distance b–a to the substrate) so that most of the ions transport to the substrate rather than undergoing dissociative recombination. The flux of radicals is then reduced. One of the advantages of LAPPS is that it is possible to control both the ion flux and neutral radical flux at the substrate.

4. Ion Transport

Many plasma-processing applications require ion bombardment of the workpiece in addition to a flow of free radicals. The physics of ion transport in LAPPS differs in important respects from the more familiar processing discharges, for several reasons: (i) The plasma is created by an external source (the electron beam) rather than by local absorption of electromagnetic energy, and ionization only occurs in a well defined spatial region. (ii) The geometrical configuration is unusual, consisting of a plasma sheet that is wide in two dimensions but narrow in the third, and typically located within a vessel of similarly large aspect ratio. (iii) The plasma transport to the workpiece is transverse to the external magnetic field, whose magnitude is such that the electrons are well magnetized but the ions are essentially unmagnetized. In this section we shall examine the ion flow to the workpiece and the vessel walls, under the conditions appropriate to LAPPS. Parts of this discussion are also applicable to other cross-field processing configurations, such as magnetically enhanced reactive ion etching (MERIE). [25,26].

4.1 The Bohm Condition in a Weakly Magnetized Plasma

In any discharge, the bulk plasma is quasineutral but adjacent to any surface there is normally a positively-charged ion-rich sheath. Within the bulk plasma, the ions are accelerated toward the surface, with the electrons maintaining quasineutrality until an abrupt transition occurs which marks the onset of the non-neutral sheath. If the quasineutral fluid equations are used to model the bulk plasma, this transition appears as a singularity in the equations [27] when the ion flow velocity component u_{ix} normal to the surface reaches the Bohm velocity, which is

$$u_{ix} = (T_e / M)^{1/2} \equiv c_s \tag{10}$$

for a single-component plasma with cold ions, where T_e is the electron temperature and M is the ion mass. The Bohm condition can be thought of as the boundary condition to the bulk flow. We shall show here that the singularity of the quasineutral fluid equations is unaffected by a weak magnetic field. We then show that an ion-rich sheath occurs in much the same way in a magnetized plasma, but that the sheath characteristics are somewhat modified if B is strong. We assume that the magnetic field **B** is uniform and take it to be in the z direction, with the plasma sheet in the yz plane and all variation in the x direction (normal to the bounding surface). The ions are represented as unmagnetized, since their gyrofrequency is small relative to the collision frequency. For electrons, the opposite is true, and both the Lorentz force and the collisional drag are included in the treatment.

In the quasi-neutral plasma the electrons and ions have equal density n, and the ion momentum equation along x is given in steady state by

$$M u_{ix} \frac{du_{ix}}{dx} = eE_x - M\nu_i u_{ix}, \tag{11}$$

where E_x is the electric field, ν_i is the ion-neutral collision frequency (primarily for charge-exchange collisions), and we assume cold ions for simplicity. For the electrons, we neglect inertia in the x component of the momentum equation, but retain the magnetic force:

$$0 = -eE_x - eB\frac{u_{ey}}{c} - \frac{T_e}{n}\frac{dn}{dx} - m\nu_e u_{ex}, \tag{12}$$

where ν_e is the electron-neutral momentum transfer collision frequency. Because of the magnetic field, an electron Hall current is driven in the y direction, governed by the momentum equation

$$mu_{ex}\frac{du_{ey}}{dx} = eB\frac{u_{ex}}{c} - m\nu_e u_{ey}. \tag{13}$$

Following the flow in x (that is from the center of the LAPPS plasma toward the substrate), Eq. (13) shows that u_{ey} rapidly asymptotes to

$$u_{ey} = \frac{\Omega_e}{\nu_e}u_{ex}, \tag{14}$$

where $\Omega_e \equiv eB/mc$ is the electron gyrofrequency. Using (12) and (14) to eliminate E_x and u_{ey}, Eq. (11) becomes

$$Mu_{ix}\frac{du_{ix}}{dx} = -\frac{T_e}{n}\frac{dn}{dx} - m\nu_e u_{ex}\left(1+\frac{\Omega_e^2}{\nu_e^2}\right) - M\nu_i u_{ix}. \tag{15}$$

To eliminate dn/dx, we use the ion continuity equation,

$$\frac{d}{dx}(nu_{ix}) = S - \beta n^2. \tag{16}$$

Equation (15) can be rewritten as

$$\frac{du_{ix}}{dx} = \frac{M\nu_i u_{ix}^2 + m\nu_e\left(1+\frac{\Omega_e^2}{\nu_e^2}\right)u_{ex}u_{ix} + \frac{T_e}{n}\left(S-\beta n^2\right)}{T_e - Mu_{ix}^2}. \tag{17}$$

Although the numerator of (17) is modified by the effect of the magnetic field on the electrons, the Bohm singularity condition, Eq. (10), arises from the denominator and is completely independent of B. When finite ion temperature is important, a more careful kinetic treatment is needed to derive a generalized Bohm condition [28], but it remains true that the effect of the magnetic field on the electrons does not modify the Bohm condition.

Equation (17) is valid in the quasi-neutral plasma up to the singular point, $u_{ix} = c_s$. In the central region where the flow velocity is very low, the term on the left hand side of Eq. (15) can be neglected. This leads to the diffusion approximation. As the plasma accelerates to the singularity, ion inertia becomes more and more important and the diffusion model breaks down. The plasma then forms a quasi-neutral presheath, typically of length of order the ion mean free path, λ_i. This presheath eventually has a transition to the non-neutral sheath when the Bohm condition is satisfied.

4.2. Cross-Field Ion Flow to an Insulating Surface

Ion flow across the magnetic field to an insulating surface is of special interest, since in most cases the workpiece to be processed will be an insulator. An insulating surface cannot sustain a steady state electric current at any point, and hence

$$n_{ex} u_{ex} = n_{ix} u_{ix} \tag{18a}$$

along this surface (assumed to be in the yz plane). If the plasma flow is one dimensional along the x axis (one dimensional across the field), then Eq. (18a) holds everywhere in the plasma as well, so in the quasi-neutral plasma, $u_{ex} = u_{ix}$. That is the plasma flow in one dimension must be ambipolar. In this case, Eq. (15) can be rewritten as

$$M u_{ix} \frac{du_{ix}}{dx} = -\frac{T_e}{n}\frac{dn}{dx} - M\nu_i^* u_{ix}, \tag{18b}$$

where

$$\nu_i^* \equiv \nu_i + \frac{m\nu_e^*}{M}, \tag{18c}$$

and

$$\nu_e^* \equiv \nu_e\left(1 + \frac{\Omega_e^2}{\nu_e^2}\right) \approx \frac{\Omega_e^2}{\nu_e}, \tag{18d}$$

since $\Omega_e >> \nu_e$. The effective mobility of the ions is reduced by the need to drag the electrons across the magnetic field. The effective ion collision frequency ν_i^* reaches a minimum at a pressure P*(B) such that

$$\nu_e \nu_i = \frac{m}{M}\Omega_e^2. \tag{19}$$

As the pressure increases above P*(B), ν_i^* increases as ion collisionality dominates; for pressure decreasing below P*(B), ν_i^* increases due to the difficulty of dragging the magnetized electrons across the field lines. In O_2 plasma, we use the values $\nu_e/n_g \sim 4\times10^{-8}T_e^{2/3}$(eV) ($cm^3$/s) [29] and $\nu_i/n_g \sim 5\times10^{-10}$ (cm^3/s) [30] nearly independent of ion temperature. Under typical LAPPS operating conditions, the magnetization of the electrons retards the ambipolar ion flow, but at most by a factor of five or so, even though the electrons are strongly magnetized.

The singularity at the Bohm condition is associated with a sudden steepening of the gradients in u_x and n, which leads to a breakdown of quasineutrality. To better understand this effect qualitatively, let us consider the simplified model of quasineutral ambipolar diffusive flow in the bulk plasma, as represented by Eqs. (18) with the inertial terms on the LHS dropped. Eliminating u_{ix} and referring back to Eq. (11), we find an expression for the ambipolar electric field,

$$eE \approx -\frac{\nu_i}{\nu_i^*}\frac{T_e}{n}\frac{dn}{dx}. \tag{20}$$

Using Gauss's law, the quasineutrality requirement $|n_i - n_e| << n$ can be written as

$$\frac{\nu_i}{\nu_i^*}\lambda_D{}^2\frac{d^2 \ln n}{dx^2} << 1, \tag{21}$$

where $\lambda_D = (T_e/4\pi ne^2)^{1/2}$ is the Debye length. Hence quasineutrality fails, and the electron and ion flows separate, once the gradient scale length becomes shorter than $\lambda_D(\nu_i/\nu_i^*)^{1/2}$. In the usual unmagnetized case, the minimum gradient scale for quasineutral flow is simply λ_D. The presence of a magnetic field transverse to the flow decreases the electron mobility and thereby increases the steepness allowed for quasineutral flow.

4.3. The Sheath for a Magnetized-Electron Plasma

Since the transition from the quasineutral bulk plasma to an ion-rich sheath can only occur at a point where the Bohm condition (10) is satisfied, it follows that the ions *must* be accelerated up to the sound speed in the quasineutral region, if there is to be an ion-rich sheath. The only other alternative is that the ion flow is entirely subsonic, and there is no sheath. In an unmagnetized plasma, it is clear that there must always be an ion-rich sheath at any floating surface, since $n_e < n_i$ is required at the surface to equalize the flux of mobile electrons and less mobile ions to the surface. One might wonder whether this is always true for flow across a magnetic field, where the mobility of the magnetized electrons can be greatly reduced. To address this question, let us return to Eq. (13) and note that within the sheath the inertial term on the left hand side dominates the collisional term, so that u_{ey} is given by

$$u_{ey}(x) = u_{ey}(x_s) + \Omega_e(x - x_s) = \Omega_e\left[\frac{c_s}{\nu_e} + (x - x_s)\right], \tag{22}$$

where x_s is the location of the sheath/plasma interface and $u_{ey}(x_s) = \Omega_e c_s/\nu_e$ from Eq. (14). Using Eq. (22) and ignoring collisions in the sheath, we can integrate Eq. (12) from the sheath edge, x_s, to obtain the electron density in the sheath,

$$\frac{n_e(x)}{n_e(x_s)} = \exp\left\{\frac{1}{T_e}\left[e[\phi(x) - \phi(x_s)] - \frac{\Omega_e^2}{\nu_e} mc_s(x - x_s) - \frac{1}{2} m\Omega_e^2 (x - x_s)^2\right]\right\}. \tag{23}$$

Equation (23) is an extension of the usual Boltzmann relation. The negative potential drop given by the first term causes n_e to fall off in the sheath. The two magnetic terms are also negative and thus the effect of the magnetic field is to further decrease n_e in the sheath. This occurs because electrons can only flow into the sheath from the plasma, and the magnetic field impedes this flow. Therefore an ion-rich sheath will indeed occur for any value of the magnetic field, and the usual Bohm condition must be satisfied at the transition from quasineutral bulk plasma to ion-rich sheath. At an insulating surface, the sheath structure and sheath potential are determined primarily by the floating condition, which requires that the ion flux to the substrate equal the electron flux. But the ion flux is $n(x_s)c_s$, since no significant ionization or recombination occurs in the sheath, while the electron flux is $n_e(b)(T_e/2\pi m)^{1/2}$ for electrons with a Maxwell-Boltzmann distribution. Thus

$$\frac{n_e(b)}{n_e(x_s)} = \sqrt{\frac{2\pi m}{M}} = \exp\left\{\frac{1}{T_e}\left[e[\phi(b) - \phi(x_s)] - \frac{\Omega_e^2}{\nu_e} mc_s(b - x_s) - \frac{1}{2} m\Omega_e^2 (b - x_s)^2\right]\right\}. \tag{24}$$

Equation (24) indicates that the sheath width $\Delta \equiv (b - x_s)$ shrinks when the magnetic terms are important. Since the width of the unmagnetized sheath is a few λ_D, the last term in (24) becomes significant when $\Omega_e > \omega_p$, where ω_p is the electron plasma frequency. The sheath width can then shrink to the order of the electron gyroradius r_e. The second term in (24) results from the transverse electron flow u_{ey} induced in the bulk plasma (which persists in the sheath due to inertia). This term is significant when $\Omega_e^2/\nu_e\omega_p > (M/m)^{1/2}$. In the usual operating regime of LAPPS these magnetic effects are small, and the sheath is effectively unmagnetized. However if n_s falls below about 10^{10} cm^{-3}, which can occur if the substrate is remote from the plasma sheet, or if the pressure is less than a few mTorr, magnetic effects can become important. In these cases, the sheath width Δ is reduced. The potential drop ϕ_s across the sheath is related to Δ by the Langmuir-Childs law governing ion flow, and thus is also smaller than the usual floating potential for an unmagnetized plasma,

$$\phi_s \le \frac{1}{2} T_e \ln\left(\frac{M}{2\pi m}\right). \tag{25a}$$

For an oxygen plasma in LAPPS, typically $\phi_s < 5$ eV. For applications such as anisotropic etching, where a much larger ion bombardment energy is needed, it is necessary to use rf bias to accelerate the ions to the substrate.

Finally if the wall is a conductor and collects current density J, the sheath potential $\phi(b)$-$\phi(x_s)$ will be determined by by

$$n(x_s)ec_s - n_e(b)e[T_e/2\pi m]^{1/2} = J, \tag{25b}$$

with $n_e(b)$ related to $\phi(b)$-$\phi(x_s)$ by Eq. (24).

4.4. Approximations to the Fluid Motion

The problem of determining the ion fluid motion can be approached at any of several levels of approximation. The most complete treatment is to integrate the complete fluid equations (11), (12), (14) and (16) from the center of the plasma up to the point x_s where $u_{ix} = c_s$. At this point the equations become singular and one patches on the sheath model described in the previous section. For zero current (floating surface), the boundary condition $u_{ex} = c_s$ also applies at x_s, and the sheath potential is determined by Eq. (25a), with an equality in the usual case where magnetic effects are unimportant in the sheath. For conducting surfaces, Eqs. (25b) and (24) are used to specify u_{ex} at x_s. This treatment includes both collisional and ion-inertial effects, and thus properly resolves both the bulk plasma (where collisions dominate) and the presheath (where ion inertia dominates). It gives an accurate expression for the potential profile across the quasi-neutral plasma.

A simpler model is to drop the ion inertia term on the LHS of Eq. (11), thereby reducing the fluid equations to diffusion equations, which are applied from the center of the plasma up to x_s. The boundary condition $nc_s = -Ddn/dx$ is then applied at x_s, and the sheath model is again patched on at that point. (Here D is the appropriate diffusion coefficient, which will be discussed at length in the next three subsections.) This approach yields an accurate result for the ion flux to the surface, provided the plasma size is large compared to the ion mean free path λ_i and the Debye length λ_D. This holds because the ion flux is simply the volumetric integral of the ionization rate less the recombination rate, and when λ_i and λ_D are small the only significant contribution to this integral is from the bulk plasma. This diffusion model will also give a good approximation to the density and potential profile within the bulk plasma, but it does not correctly describe these quantities in the presheath, i.e. the last ion mean free path before x_s.

A still simpler approximation is to use the diffusion model right up to the bounding surface at x = b, and apply the boundary condition n = 0 at b. The flux to the surface is then given by –Ddn/dx, and it is not necessary to use the Bohm condition as a boundary condition to

the fluid equations. If the plasma size is large compared to λ_i and λ_D, and $n(x_s)$ is much less than the central density, this simple model gives a good approximation to the ion flux to the surface, and also to the density and potential profile within the bulk plasma, but it does not correctly describe the presheath and it completely omits the potential drop in the sheath. As we shall see in the next subsection, it also has the advantage of reducing the dimension of the parameter space which characterizes the solutions.

4.5. One Dimensional Diffusion Model for LAPPS

LAPPS differs from other plasma sources in that essentially all of the ionization occurs in a well-defined source region $-a \le x \le a$, determined by the thickness of the sheet electron beam. It is a very broad plasma, essentially forming a sheet. For processing, a substrate will be placed adjacent to the plasma, but outside the source region, so as to avoid bombardment by the beam. Since the plasma sheet is very broad, the configuration is very nearly one dimensional, with variation mainly in the dimension x, perpendicular to the plasma sheet. Thus we begin our calculations of ion transport in this section with a one dimensional diffusion model. In the next two sections, we shall extend the model to two dimensions, to address the issue of uniformity along the magnetic field.

The LAPPS plasma consists of the source region as well as a transport region $a \le x \le b$, where b is the substrate location. For simplicity, we shall assume a symmetric situation with identical substrates on each side of the plasma sheet at $\pm b$. A schematic illustration of the typical plasma density profile is shown in Fig. 3. One of the advantages of LAPPS is that the ion flux to the substrate depends on the values of a, b, J_b, the gas pressure P, and the gas species (because recombination is important for molecular gases, but not for atomic gases). By adjusting one or more of these variables, one can control the ratio of ion flux to neutral radical flux, over a wide range.

Since we assume $b >> \lambda_i$, the central density is much larger than the edge density, and because we are most interested in central density and edge flux, we use a diffusion model with the boundary condition that the density vanishes at the wall. The ambipolar diffusion coefficient is given according to earlier analysis by

$$D_a = \frac{T_e}{M\nu_i^*} \equiv \frac{T_e}{M\nu_i + m\nu_e^*} \,. \tag{26}$$

With this approximation, Eq. (16) reduces to a diffusion equation which also includes recombination and (in the region $-a \le x \le a$) ionization,

$$D_a \frac{d^2 n}{dx^2} = \beta n^2 - S, \qquad \text{for } 0 \le x \le a, \tag{27a}$$

$$D_a \frac{d^2 n}{dx^2} = \beta n^2, \qquad \text{for } a \le x \le b. \tag{27b}$$

Attachment can be ignored in oxygen because the electron temperature and gas density are both low in LAPPS. As boundary conditions we take

$$n(b) = 0 \tag{28}$$

and

$$\left.\frac{dn}{dx}\right|_{x=0} = 0, \tag{29}$$

and of course continuity of n and its derivative at x = a. The ion flux F_i is given by

$$F_i(x) = -D_a \frac{dn}{dx} \tag{30}$$

and we are especially interested in this flux at x=b.

In Appendix A, we discuss the solution of Eqs. (26-30) in detail. There, we define dimensionless parameters, by scaling the density to

$$n_o = \sqrt{S/\beta} \tag{31a}$$

the length to

$$x_o = \left[\frac{D}{\sqrt{\beta S}}\right]^{1/2} \tag{31b}$$

and the flux to

$$F_o = D\frac{n_o}{x_o} \tag{31c}$$

Here n_o is the density as specified by balancing the ionization source against recombination. The density of a LAPPS plasma is always less than n_o, since diffusion only reduces n. The length x_o is the distance an ion diffuses in a recombination time $(\beta n_o)^{-1}$. The dimensionless variables are now $N \equiv n/n_o$, $X \equiv x/x_o$ and $F \equiv F_i/F = -dN/dX$.

It then turns out that there are only two dimensionless parameters which characterize the solution, $A = a/x_o$, and $B = b/x_o$. There are four parameter regimes, shown in Fig. (4), in which one can derive approximate analytic solutions based on A and B-A being either large or small. The dimensionless results for central density N_0, and flux F_B at the wall X=B, in each of the four regimes are derived in Appendix A and summarized here. We find:

Regime 1 (small A and small B-A), no recombination in either the source or transport region:

$$N_0 = AB + \tfrac{1}{2}A^2, \qquad F_B = A \tag{32a}$$

Regime 2 (large A, small B-A), recombination dominated in the source region, but the substrate close to the source:

$$N_o \simeq 1 \qquad F_B \cong \frac{\sqrt{2}}{\sqrt{2}(B-A)+\coth(\sqrt{2}A)} \tag{32b}$$

Regime 3 (small A, large B-A), no recombination in the source region, but recombination is important in the transport region to the substrate:

$$N_0 = \left(\frac{3}{2}\right)^{1/3} A^{2/3} + \tfrac{1}{2}A^2, \qquad F_B = \frac{35}{(B-A)^3}. \tag{32c}$$

Regime 4 (large A, large B-A), recombination dominant in both the source and transport region:

$$N_o \simeq 1, \qquad F_B = \frac{35}{(B-A)^3}. \tag{32d}$$

If the objective is to maximize the ion flux, then N_o should be as close to unity as possible, and B-A should be as small as possible, so as to minimize recombination outside the source region.

In Regime 1, where recombination is not significant, every ion created in the source region $0 \le x \le a$ reaches the substrate, and thus the ion flux is proportional to the product of the source strength S and the source width a. In this regime, the neutral flux is due entirely to direct dissociation of molecules by the beam, and thus is smaller than the ion flux. If the objective is to maximize the ion flux, one can locate the substrate immediately adjacent to the source region (B–A<<1) and increase S and/or a. However either of these changes increases A so that the parameters eventually fall in Regime 2. In this regime, the ion density at x=0 reaches its recombination-limited value (31a), and the neutral radical flux to the substrate is augmented by dissociative recombination in the source region. If the objective is to minimize ion flux to the substrate and maximize neutral radical flux, the separation b–a of the substrate from the source region can be increased, so that the parameters fall into Regime 3 or 4. Here the ion flux is

independent of the source strength S but falls off as the inverse cube of the offset b–a. In this regime, the neutral radical flux is proportional to the source strength and independent of b–a, since nearly all ions produced in the source region undergo dissociative recombination, creating free radicals which reach the substrate. Because all of the ionization occurs in a very well defined source region, LAPPS thus provides the capability to very effectively adjust the ratio of ion flux to free-radical flux by choosing appropriate values of I_b, the beam current, and B–A, the standoff distance, as well as the gas.

4.6. Two Dimensional Diffusion Model for LAPPS, Insulating Boundary

In this section we begin our study of uniformity of ion flux to the substrate. To investigate non-uniformities in the z-direction (along the magnetic field, where we expect end effects to be most significant), we extend the diffusion model of the previous section to two dimensions x and z, with x the direction normal to the substrate. We assume that the LAPPS plasma occupies a region $-b \le x \le b$, $-L \le z \le L$, with $b \ll L$. In the present section we pay careful attention to the boundary conditions on the potential $\phi(x,z)$, but we simplify the problem a bit by ignoring recombination and setting b = a so that the collectors are located right at the edge of the beam. More complete numerical studies will be presented in future work. The 2-D electron and ion momentum equations (with inertia dropped) and the continuity equation are

$$m\underline{\underline{\nu}}_e^* \cdot \mathbf{u}_e = e\nabla\phi - \frac{T_e}{n}\nabla n, \tag{33}$$

$$M\nu_i \mathbf{u}_i = -e\nabla\phi \tag{34}$$

$$\nabla \cdot n\mathbf{u}_e = \nabla \cdot n\mathbf{u}_i = S \tag{35}$$

where the anisotropic diagonal tensor $\underline{\underline{\nu}}_e^*$ has component ν_e in the z-direction (along the field), but $\underline{\underline{\nu}}_e^* \equiv \nu_e(1+\Omega^2/\nu_e^2) \equiv \Omega_e^2/\nu_e$ in the x-direction (across the field). For LAPPS parameters, $\Omega_e \gg \nu_e$ and thus the electron parallel mobility greatly exceeds the transverse mobility. Using Eqs. (33) and (34) to eliminate $\mathbf{u}_i$ and $\mathbf{u}_e$ from Eqs. (35) gives two coupled equations for n and ϕ,

$$\nabla \cdot n\nabla\left(\frac{e\phi}{M\nu_i}\right) = -S, \tag{36a}$$

$$\nabla \cdot n\underline{\underline{\nu}}_e^{*-1}\left(\frac{e}{m}\nabla\phi - \frac{T_e}{mn}\nabla n\right) = S. \tag{36b}$$

Note that we have not invoked the ambipolar assumption $\mathbf{u}_e = \mathbf{u}_i$. These coupled Poisson type equations for n and ϕ can be solved if n and ϕ or their normal derivatives are specified on the bounday.

The analysis of Eqs. (36) is complicated by the fact that these equations apply only in the quasineutral bulk plasma, and thus require boundary conditions at the interface between the bulk plasma and the sheath, rather than at the wall itself. The boundary condition on the normal derivative $\nabla_\perp \phi$ is specified by the Bohm condition that the ion velocity normal to the wall be equal to the ion sound speed c_s. Together with Eq. (34), this gives

$$e\nabla_\perp \phi = -M\nu_i c_s \,. \tag{37}$$

The boundary condition on $\nabla_\perp n$ derives from the electron flow and depends on whether the wall is insulating or conducting. In the remainder of this section, we study this boundary value problem for the case of an insulating substrate, which is the usual case in plasma processing (and also the the simpler case to analyze). Ion flow to a conductor will be considered in the next section and in Appendix B. Fortunately, we find that end effects are minimal for insulating substrates. In fact, if a conductor is to be processed, uniformity is optimized by placing it on an insulator to electrically isolate it from the rest of the circuit.

At an insulating surface, the boundary condition on $\nabla_\perp n$ follows from the floating condition that there be no electrical current into the wall at any point. Hence, at the plasma-sheath interface the normal electron velocity $\mathbf{u}_{e\perp}$ must be equal to the normal ion velocity $\mathbf{u}_{e\perp}$, which we know to be c_s. Using the electron momentum equation (33), we find that the boundary condition at the sheath interface on the side wall ($x=\pm b$) is

$$n\left(m\nu_e^* + M\nu_i\right)c_s = -T_e \frac{\partial n}{\partial x} \tag{38a}$$

and at the end wall ($z=\pm L$) is

$$n\left(m\nu_e + M\nu_i\right)c_s = -T_e \frac{\partial n}{\partial z} \tag{38b}$$

One might think that the electron and ion velocities must be equal everywhere, since there is no current to the wall at any point. However this is not generally true. Equation (34) shows that $\mathbf{u}_i$ is the gradient of a scalar, whereas Eq. (33) shows that $\underline{\underline{\nu}}_e^* \cdot \mathbf{u}_e$ is the gradient of a scalar. It follows that $\mathbf{u}_e$ and $\mathbf{u}_i$ cannot be equal everywhere unless the tensor $\underline{\underline{\nu}}_e^*$ is a scalar, or the density is separable in the form $n(x,z)=n^{(1)}(x)\, n^{(2)}(z)$. Neither condition is satisfied in general, although the latter is very nearly true when $b \ll L$. Furthermore, in a multi-dimensional anisotropic plasma, it is not possible in general to decouple n and ϕ so that one can write a simple diffusion equation for n.

As a preliminary to the 2-D analysis, we re-examine the 1-D cross-field diffusion problem ($L\to\infty$) with an emphasis on understanding the profiles of both n and ϕ. In one dimension, quasineutrality does require $u_e=u_i$, and as noted in Sec. 4.5 it follows that n satisfies an ambipolar diffusion equation with diffusion coefficient D_a given by E. (26). The solution to this equation, in the present context with b=a, no recombination, and with boundary condition (38a) is

$$n^{(1)} = n_o - \frac{S(M\nu_i + m\nu_e^*)}{2T_e}x^2 \tag{39a}$$

and

$$n_o = \frac{S(M\nu_i + m\nu_e^*)}{2T_e}b^2 + \frac{Sb}{c_s} \tag{39b}$$

Equations (33) and (34) can be solved for ϕ:

$$\frac{e(\phi^{(1)} - \phi_0)}{T_e} = \frac{M\nu_i}{M\nu_i + m\nu_e^*}\ln\left(\frac{n^{(1)}}{n_0}\right). \tag{40}$$

where ϕo is the potential in the center of the plasma. The superscripts (1) denote 1-D dependence in the x-direction. Notice that the relationship between ϕ and n is similar to the Boltzmann relation, except that the coefficient multiplying the logarithm is less than unity, and for strongly magnetized electrons, may be considerably less. For typical LAPPS parameters, this coefficient may vary between about 0.1 and 0.5. If the flow is strongly inhibited by the magnetization of the electrons, Eq. (40) shows that the potential drop between the center and the edge of the quasineutral plasma is reduced. We showed in Sec. 4.3 that the sheath potential drop is also reduced by the presence of the magnetic field; although usually only slightly. Hence the total potential drop from the central plasma to the wall is reduced by the magnetic field.

Now let us examine how this solution is modified by the additional boundaries at $z=\pm L$. Since elliptic equations are stable to small perturbations of the boundary conditions, we do not expect that adding finite boundaries at $z=\pm L$ will have a large effect on the solution away from the ends. We shall derive an approximate solution which shows explicitly that for LAPPS geometry with $b<<L$, the one-dimensional solution is very nearly correct except in the immediate vicinity of the end walls (within a distance of a few times b).

The set of equations (36) is not exactly separable in x and z. However, we take advantage of the high aspect ration ($b<<L$) to write an ansatz in the separated form

$$n(x,z) = n^{(1)}(x)n^{(2)}(z) \equiv n^{(1)}(x)\left[\exp\left(\frac{e\phi^{(2)}}{T_e}\right) + \varepsilon(z)\right], \tag{41a}$$

$$\phi(x,z) \equiv \phi^{(1)}(x) + \phi^{(2)}(z). \tag{41b}$$

In addition to separating variables x and z in n(x,z), we have assumed that the x-dependence of n and ϕ is close to the 1-D solutions $n^{(1)}(x)$, $\phi^{(1)}(x)$ from Eqs. (39) and (40), we have anticipated a logarithmic relation between ϕ and n to write $\phi(x,z)$ in an additively separated form, and we have written the density dependence $n^{(2)}(z)$ along the magnetic field as a Boltzmann factor plus a correction $\varepsilon(z)$; we shall show explicitly that $\varepsilon(z)$ is small. Inserting Eqs. (41) into (36), we find that the x-dependence mostly cancels out of the equations, validating the assumptions made in the ansatz. In places where there is a remaining dependence on x, we simply evaluate it at x=0. We expect that this procedure will preserve the qualitative properties of the solution. After making one additional well-justified approximation, dropping the last term of (39b) which is small when the density at the sheath interface is much less than the central density n_0, Eqs. (36) reduce to two coupled ordinary differential equations for $\phi^{(2)}(z)$ and $\varepsilon(z)$,

$$\exp\left(\frac{e\phi^{(2)}}{T_e}\right) + \varepsilon - 1 = \frac{1 + \frac{m\nu_e^*}{M\nu_i}}{2} b^2 \frac{\partial}{\partial z}\left\{\left[\exp\frac{e\phi^{(2)}}{T_e} + \varepsilon\right]\frac{\partial}{\partial z}\frac{e\phi^{(2)}}{T_e}\right\} \tag{42a}$$

$$\exp\left(\frac{e\phi^{(2)}}{T_e}\right) + \varepsilon - 1 = \frac{b^2}{2}\frac{\nu_e^*}{\nu_e}\frac{\partial^2}{\partial z^2}\varepsilon \tag{42b}$$

Equation (42b) can be integrated, using the boundary conditions $\varepsilon(0)=\phi^{(2)}(0)=0$, to yield an algebraic relation between $\varepsilon(z)$ and $\phi^{(2)}(z)$,

$$\varepsilon = \frac{\nu_e}{\nu_e^*}\left[1 + \frac{m\nu_e^*}{M\nu_i}\right]\left[-1 - \frac{e\phi^{(2)}}{T_e} + \exp\left(\frac{e\phi^{(2)}}{T_e}\right)\right] \tag{43}$$

For a strongly magnetized plasma, $\nu_e/\nu_e^* << 1$, and thus $\varepsilon<<1$ as anticipated. Neglecting $\varepsilon(z)$, Eq. (41a) reduces to the Boltzmann relation

$$n^{(2)}(z) = \exp\left(\frac{e\phi^{(2)}(z)}{T_e}\right), \tag{44}$$

and Eq. (42a) reduces to

$$\tilde{b}^2 \frac{d^2 n^{(2)}}{dz^2} = n^{(2)}(z) - 1, \tag{45a}$$

where

$$\tilde{b} \equiv b\sqrt{\frac{M\nu_i + m\nu_e^*}{2M\nu_i}}. \tag{45b}$$

The solution to Eq. (45a) with boundary condition (38b) is

$$n^{(2)}(z) = 1 - \frac{\tilde{b}\nu_i}{\tilde{b}\nu_i + c_s \coth\left(L/\tilde{b}\right)} \frac{\sinh\left(z/\tilde{b}\right)}{\sinh\left(L/\tilde{b}\right)}. \tag{46a}$$

Equation (44) then gives

$$\frac{e\phi^{(2)}(L)}{T_e} = \ln\left(\frac{c_s}{c_s + \tilde{b}\nu_i}\right). \tag{46b}$$

Equation (45) indicates that the end effects are felt only in the immediate vicinity of z=±L. Under typical LAPPS conditions, $\tilde{b}$ is about 3b, or about 3 cm. The plasma density is uniform to within 1% for $|z| < L - 5\tilde{b}$, and to the same accuracy the ion flux to the substrate is uniform and given by 1-D ambipolar flow. To avoid end effects and maintain uniformity of processing, it is only necessary to specify that the substrate be smaller than the plasma length L by about $5\tilde{b}$, i.e. in a typical LAPPS system with L=100 cm, the substrate size could be up to 70 cm.

Note that the densities at x=b and z=L are related by $n(z=L)/n(x=b) \approx \left[\left(M\nu_i + m\nu_e^*\right)/2M\nu_i\right]^{1/2}$. Therefore the difference in potential between x=b and z=L (the side wall and end wall) is dominated by the coefficients of the logarithm in Eqs (40 and 46b). The end walls float at a more negative potential than the side walls. This potential difference develops to inhibit the free flow of the electrons along the magnetic field. For typical LAPPS parameters, this potential difference turns out to be less than the electron temperature, i.e. less than about half a volt.

4.7. Two Dimensional Diffusion Model for LAPPS, Conducting Boundary

If the bounding surfaces are conductors, electric current can flow from the plasma to points on the boundary, but of course the total electric current flowing out of the plasma must be zero in steady state. If the walls are grounded, one may anticipate a tendency for the ion current to the side walls to be balanced by electron current along the field to the end walls, since the electron mobility is much greater along the magnetic field. In fact, the last subsection showed that for zero wall current, the end wall floats down to a lower potential than the side wall. Correspondingly, if the entire surface is grounded, current would flow from the end wall to the side wall.

However, the boundary may consist of electrically isolated conducting regions biased to different potentials, and this strongly influences the plasma current flow pattern. For example, if the end walls are biased slightly negative with respect to the side walls, to exactly the level discussed in the previous section for insulating boundaries, then the plasma can be forced into an ambipolar diffusion pattern (with zero electric current) similar to that which occurs for insulating boundaries. If, on the other hand, the side walls are biased strongly negatively with respect to the end walls, then energetic ion bombardment of the side walls will occur, with all of the electron flow to the end walls. A dc-biased configuration of this type might be used to process a conducting substrate, and it is also of interest in connection with one of the initial experiments performed at NRL. A general analysis is quite complicated and will not be attempted in this paper, but we shall outline the physical principles that govern the density, potential and flow within the plasma and sheath, and then proceed to a special case where an analytic solution is available.

The conducting boundary case is governed (within our diffusion approximation) by the same two equations (36a and b) that applied to the insulating case, and the Bohm boundary condition (37) also applies to both cases. However the complexities of the conducting case arise from the electron flow, which is reflected in the other required boundary condition. We recall that Eqs. (36a and b) apply only in the quasineutral plasma, and therefore a boundary condition is needed on the sheath-plasma interface. Such a condition must be inferred from the control parameter in an experiment, which is normally the potential ϕ_w on the conducting surfaces. Let us assume the end walls are grounded, and consider first the case where the side wall is biased to a potential $\phi_w << -T_e$, so negative that electron current to that wall is suppressed. Then there must be no electron flux into the sheath, and Eqs. (33) and (38) indicate that the appropriate boundary condition at the sheath-plasma interface on the side wall is

$$\frac{T_e}{n}\frac{\partial n}{\partial x} = e\frac{\partial \phi}{\partial x} = -M\nu_i c_s . \qquad (47)$$

Within the plasma, the electron current in the x-direction may not be exactly zero, as it is on the interface, but if there is any electron current it should be in the outward direction. Thus

$$e\frac{\partial\phi}{\partial x} < \frac{T_e}{n}\frac{\partial n}{\partial x}, \tag{48}$$

and the potential drop from the plasma center to the interface should be no more than a few times T_e. The potential drop ϕ_s across the sheath at the side wall will be nearly equal to ϕ_w, and since the sheath is free of electrons, the ion current to the wall is determined by the Langmuir-Childs ion diode equation, which for O_2^+ ions is

$$J(A/cm^2) \equiv nec_s = 1.1x10^{-8}\frac{V^{3/2}(volts)}{s^2(cm)} \tag{49}$$

The potential drop from the plasma center to the end wall is determined by the requirement that the electron current to the end wall be equal to the ion current to the side wall, and this ensures that the plasma floats at a slightly positive potential, of the order of T_e.

If the side walls are grounded or biased to a small negative potential (of the order of T_e), there will be some electron current J_{ex} flowing from the plasma to the side wall, but because of the electron mobility anisotropy, J_{ex} will be less than the ion current J_{ix}. The sheath potential at the side wall is determined by the requirement that the electron current arriving at the sheath from the plasma be equal to the electron current penetrating the sheath potential barrier to arrive at the wall. The remaining electron current flows to the end wall, and as in the previous case the plasma potential floats at a slightly positive value determined by the requirement that the total electron current to the walls be equal to the ion current.

As noted above, a slight positive bias of the side walls can lead to equal electron and ion flux to these walls, i.e. zero electric current to the side walls.

A complete mathematical formulation of these concepts would depend on the solutions to Eqs. (36a and b) subject to the appropriate boundary conditions. This is a rather complex problem, because up to this point we have considered boundary conditions on the current, but for the conducting wall it is the potential which is specified along the wall. Furthermore, depending on the current density along the sheath edge, an equipotential sheath edge does not necessarily imply the wall is an equipotential (See Eq. (25b)). However the problem simplifies if we consider the case of side walls negatively biased to such a low potential that electron current is completely cut off. Then, even if the potential along the sheath edge turns out to vary, this variation can be compensated by a variation of the sheath potential such as to set the side wall to an equipotential. Thus the ion current along the sheath edge is nec_s at each point. Since the sheath current and voltage are related by Eq. (49), there may be a slight variation in sheath voltage and sheath width along the side wall.

For the case of the strongly negatively biased side wall, simplifications occur if we additionally restrict ourselves to situations where (i) the electron friction along the magnetic field makes a negligible contribution to the total electron momentum equation, and (ii) the

magnetic field is sufficiently large that the electron cross field motion is suppressed. In that case, the Boltzmann relation

$$\frac{e(\phi-\phi_0)}{T_e}=\ln\left(\frac{n}{n_0}\right) \tag{50}$$

holds everywhere in the plasma, and Eqs. (34) and (35) reduce to a simple scalar diffusion equation

$$\nabla\cdot\frac{T_e}{M\nu_i}\nabla n=-S, \tag{51}$$

where the diffusion coefficient is equal to the ion diffusion coefficient for an *unmagnetized* plasma. In this case, the potential drop from the plasma center to the plasma-sheath interface is larger than is the case for one-dimensional magnetized-ambipolar flow, discussed previously. An approximate Green's function analysis of Eq. (51), keeping only the single term in the expansion in x which corresponding to the maximum wavelength, leads to the approximate solution

$$n=-\frac{16Sb^2}{\pi^3 D_{xx}\sinh(\pi L/b)}\left[-\sinh\frac{\pi(L-z)}{2b}\left(\cosh\frac{\pi(L+z)}{2b}-1\right)\right.$$
$$\left.+\sinh\frac{\pi(L+z)}{2b}\left(1-\cosh\frac{\pi(L-z)}{2b}\right)\right]\sin\frac{\pi(x+b)}{2b} \tag{52}$$

which shows that the flow to the side wall is uniform to within 1%, everywhere within the range $-(L-3b) < z < (L-3b)$, i.e. to within a few cm of the end plates. However, we show in Appendix B that the validity condition for assumption (i) is that

$$\frac{L}{b}\ll\sqrt{\frac{M\nu_i}{m\nu_e}}, \tag{53a}$$

and the validity condition for assumption (ii) is

$$\frac{L}{b}\ll\frac{\Omega_e}{\nu_e}. \tag{53b}$$

In LAPPS, it is always true that $L/b \gg 1$, but Eqs. (53) show that this solution applies only when L/b is not *too* large. The solution does apply reasonably well to an experiment which is discussed in the next section, but not to the larger aspect ratios planned for LAPPS applications. In situations where Eqs. (53) do not hold, we do not expect the plasma density or ion flux to be uniform in z. In processing large conducting substrates, we anticipate that it would be

advantageous to electrically isolate the substrate, so as to restore the excellent uniformity which LAPPS provides for insulating surfaces.

5. Comparison with Experiment

A preliminary experiment was performed to explore the nature of ion flow to a substrate placed parallel to the plasma sheet. Although the experiment was performed with a minimal set of diagnostics, the results are of interest and will be reported here.

The experimental apparatus is shown in Fig. 5. In oxygen at pressure 50 to 65 mT, a discharge was drawn from a slotted hollow cathode 2 cm wide × 15 cm long to a grounded anode 20 cm away. The cathode was pulsed to voltage −1 kV for a duration of 200 μsec. A slot 1.25 cm wide × 6.25 cm long was cut into the anode, allowing a beam of energetic electrons, guided by a 70 G magnetic field, to pass through the anode into a grounded chamber which we call the "toaster." The discharge current was 7 A, but the fraction of the discharge current which was carried by the electron beam and thus penetrated into the toaster was not measured. However, these beam electrons originate as secondaries emitted by the surface of the hollow cathode under ion bombardment. Normally the secondary emission coefficient is about 10%, and one therefore expects (in agreement with previous measurements on similar hollow cathode sources) that about 10% of the discharge current will be carried by the beam. The beam current density is thus expected to be about 30 mA/cm^2. The beam ionized the gas in the toaster to create a plasma sheet there. Two metal collector plates were placed inside the toaster, one on each side of the plasma sheet. Collector 1 was located at $x=b_1=a+0.6$ cm, and Collector 2 at $x=b_2=a+1.0$ cm, with $a\cong 0.62$ cm the half-width of the beam. The entire apparatus was enclosed in an acrylic pressure vessel, and the plasma was visible from the sides. The collectors were dc-biased to the same negative bias ϕ_{bias}, which was varied in steps of 10 V from 0 to −120 V, and the currents $I_1(t)$ and $I_2(t)$ to each of the collectors were measured over the duration of the discharge.

Key observations include the following. (i) At zero bias, the steady state values of I_1 and I_2 are zero. (ii) For all cases with negative bias, $I_1(t)$ and $I_2(t)$ are positive and after ~40 μsec reach values I_1 and I_2 which are essentially steady state. (iii) The dependence of I_1 and I_2 on ϕ_{bias} is shown in Fig. 6. I_1 and I_2 have large positive values at $\phi_{bias} = -10$ V, the first measured value of negative bias, and then I_1 and I_2 increase slowly (by roughly a factor of two) as $-\phi_{bias}$ increases to 100 V. At this point, I_1 and I_2 appear to saturate. For $\phi_{bias} < -120$ V, there was visual evidence of an additional discharge striking from the collector plates. (iv) As the pressure increases with ϕ_{bias} held constant at −30 V, I_1 and I_2 fall off as shown in Fig. 7. (v) The ratio I_1/I_2 was ~0.75 in all cases.

We now consider the interpretation of these data in light of the simple model developed in Secs. 4.5 - 4.7. For the parameters of these experiments, with L = 15 cm, inequalities (47) are satisfied, so we apply the model developed in Sec. 4.7.

As seen in Sec. 4.6, a slight positive bias of the side collectors (relative to the end walls) is sufficient to draw electron current, equal and opposite to the ion current, to the collectors. For the parameters of the present experiment, this bias is only 0.3 V. Hence, we expect essentially zero electrical current to the collectors when they are at the same potential as the end walls. This is in agreement with the experiment.

When the collectors are biased to negative voltage greater than a few times T_e, the theory predicts that a uniform ion current, specified by the diffusion equation, Eq. (51) for unmagnetized ions, will flow to the collector surfaces, and electron current will flow only to the end walls. T_e was not measured in this experiment, but a theoretical calculation indicates that T_e should be about 0.5 V, and a subsequent LAPPS experiment [21] measured T_e=0.6 V in a similar oxygen plasma. Thus one expects the ion current to the collectors to be at its saturated value for all of the measured cases with negative bias, since $\phi_{bias} \leq -10$ V in all of these cases. However, the experiment showed a slow increase in collector current as $-\phi_{bias}$ increased from 10 V to 100 V.

The current to the negatively biased collectors is determined not only by the Bohm condition, but even more fundamentally, by the plasma production rate. The increase in ion current with bias voltage appears to indicate an increase in plasma production rate. We believe that the explanation for this is as follows. Ion bombardment of the collectors liberates electrons from the surface. For most metals, the efficiency of this process is about 0.1 electrons per ion, rather insensitive to the ion energy in the range 10 eV to several hundred eV [31]. These electrons are then accelerated through the sheath into the plasma, where they can ionize the gas if their energy is high enough. At bias voltage –10 V, less than the ionization potential of O_2, no secondary ionization can occur, and the secondary electrons have no effect on the ion current to the collector. Thus we expect that the measured collector currents at $\phi_{bias} = -10$ V are a faithful representation of the ion flow from the beam-generated LAPPS plasma. However, as $-\phi_{bias}$ increases above 12V, the cross-section for ionization by the secondary electrons increases, reaching a maximum when $-\phi_{bias}$ = 120V. Even at 100V, the voltage is not sufficient for a self-sustaining cathode fall [32], so the collector bias will not control the discharge. Nevertheless, the additional ionization can substantially increase the ion density near the sheath, and thus (according to the Bohm condition) the ion flux to the collectors. Indeed, secondary discharges are visible near the collectors when $-\phi_{bias} \geq$ 100V.

The data on pressure scaling of the collector current was taken at bias –30 V, where there is no more than a moderate effect from secondary ionization. To interpret this data, we use the unmagnetized scalar diffusion equation (51). As discussed in Sec. 4.7, this diffusion process results in very nearly one-dimensional uniform flow, except for small regions at the ends. Thus we may apply the one-dimensional diffusion/recombination theory developed in Sec. 4.5, using however the unmagnetized-ion diffusion coefficient $D_i=T_e/M\nu_i$ rather than the ambipolar diffusion coefficient (26). The geometry of the experiment is not quite symmetric in x, as

assumed in the theory, since the offsets b_1 and b_2 are different, but we simply apply the theory to each collector with its own value of b. With all of these simplifications, we may list the scaling of the various quantities characterizing the plasma and the ion flow to the substrate, in terms of P in torr and T_e in eV: ionization source $S = 1.8\times10^{18}P$ $cm^{-3}s^{-1}$, recombination coefficient $\beta=2.5\times10^{-8}T_e^{-1/2}$, diffusion coefficient $D_i=1.7\times10^{3}T_eP^{-1}$ $cm^{-3}s^{-1}$, characteristic density [Eq. (31a)] $n_0=8\times10^{12}P^{1/2}T_e^{1/4}$ cm^{-3}, characteristic length [Eq. (31b)] $x_0=9\times10^{-2}T_e^{5/8}P^{-3/4}$ cm, characteristic ion flux $F_0=D_in_0/x_0$ $cm^{-2}s^{-1}$. The two dimensionless parameters characterizing the diffusion/recombination process are A=1.4, and B–A=1.4 for Collector 1, B–A=2.3 for Collector 2. In both cases, the parameters fall into Regime 2 defined in Appendix A, and shown in Fig. 4, where the dimensionless ion flux is given by Eq. (A11). Multiplying the dimensionless flux by the characteristic flux F_0, the electron charge, and the area (36 cm^2), we find the predicted current to the collector to be

$$I=\frac{8\times10^{-2}T_e^{5/8}P^{-1/2}}{b-a+6\times10^{-2}T_e^{5/8}P^{-3/4}\coth\left(9T_e^{5/8}P^{-3/4}\right)}\ \text{Amps}, \qquad (54)$$

where a and b are in cm. Normalizing the current predicted by Eq. (54) to the measured current to Collector 2 at P = 60 mTorr, we find $T_e\cong0.4$ eV, in reasonable agreement with theoretical predictions and evidence from other LAPPS experiments. Using this value for T_e in Eq. (54), the predicted currents $I_1(P)$ and $I_1(P)$ are compared to the measured currents in Fig. 7. The agreement is quite reasonable, given the many approximations and simplifications in the theory, and the preliminary nature of the measurements.

6. Summary

In this paper we have discussed the key features of LAPPS and found that it offers significant improvements in performance over other plasma reactors. Benefits include (i) high uniformity over large area (up to and exceeding 1 m^2); (ii) high efficiency; (iii) independent control of ion and radical fluxes to substrates; (iv) wide operating range in gas type and pressure; and (v) low and externally adjustable plasma temperature. Unlike other reactors, LAPPS uses an electron beam of several keV to ionize and dissociate the constituent gases. As a result, the primary control parameters are the beam current, the standoff distance from beam to substrate, and the gas type and pressure. No other plasma source is known to offer a similar degee of control, flexibility, and efficiency over such a large area. Nevertheless, LAPPS does have disadvantages, including the tradeoff between efficiency and uniformity (depending on usage and whether beam energy is recovered), the need for a beam source, and the need for a magnetic field (~200 G) to confine the beam. However efficient beam sources are now available and are being developed for LAPPS. Also, we have found that the magnetic field has little effect on ion transport in LAPPS.

A comparison of a preliminary experiment on LAPPS with theory showed good agreement, and more extensive experiments are now comoing on line. [16,17, 21,33,34]. These experiment use an advanced hollow cathode source [15] which is efficient and can operate pulsed or cw to produce meter sized plasmas. Results so far have been on pulsed plasmas with smaller area. Diagnostics include a Langmuir probe to measure electron density, electron temperature and plasma potential, an X band microwave interferometer to measure line average electron density, and a mass spectrometer to measure ion mass and energy. Future upgrades will include laser induced fluorescence. While the preliminary experiment we have analyzed was for dc bias, etching experiments, will be done with rf bias [17]. An initial theory of sheaths with rf bias in a LAPPS plasma is also underway [35, 36].

Appendix A, Approximate Analytic Solutions a One Dimensional Plasma

We consider here approximate analytic solutions for Eqs. (26-30). We begin by writing these in dimensionless form

$$N'' + 1 - N^2 = 0, \quad \text{for } 0 \le X \le A, \tag{A1a}$$

$$N'' - N^2 = 0, \quad \text{for } A \le X \le B, \tag{A1b}$$

$$N'(0) = 0, \tag{A2a}$$

$$N(B) = 0, \tag{A2b}$$

where $N=n/n_o$, $X=x/x_o$ and a prime denotes d/dX. We shall also use the notation subscript-A for the value of a variable at X=A, subscript-B for X=B, and subscript-0 for X=0. Equations (A1) can be solved by quadrature. Integrating (A1a) twice from 0 to X and applying the boundary condition (A2a), we find

$$X = \int_{N(X)}^{N_0} \frac{d\tilde{N}}{\sqrt{2\left[N_0 - \tilde{N}\right] - \frac{2}{3}\left[N_0^3 - \tilde{N}^3\right]}}. \tag{A3}$$

Integrating (A1b) from X to B gives the useful relation

$$N'^2 = N_B'^2 + \tfrac{2}{3}N^3, \text{ or equivalently } \quad F^2 = F_B^2 + \tfrac{2}{3}N^3, \tag{A4a}$$

where F_B is the dimensionless flux at the wall. Integrating again gives

$$B - X = \int_0^{N(X)} \frac{d\tilde{N}}{\sqrt{F_B^2 + \frac{2}{3}\tilde{N}^3}}. \tag{A4b}$$

Equations (A3) and (A4) indicate that N(X) peaks at X=0 and falls off monotonically with increasing X, as might be expected. The solution for N(X) and F_B can be obtained by requiring continuity of N(X) and N'(X) at $X = A$. Instead of proceeding numerically to a general solution, we shall consider separately analytic approximations in each of the four limiting regimes with A large or small and A-B large or small.

Regime 1: Recombination insignificant in both source and transport regions (A and B small)

If recombination can be neglected, i.e. the term N^2 is small, Eqs. (A1) reduce to a simple diffusion equation for which the solution is

$$N(X) = N_0 - \tfrac{1}{2}X^2, \qquad 0 \le X \le A, \tag{A5a}$$

$$N(X) = N_A \frac{B-X}{B-A} = (B-X)F_B, \qquad A \le X \le B. \tag{A5b}$$

Requiring continuity of N′ at A, we find the central density to be

$$N_0 = AB + \tfrac{1}{2}A^2, \tag{A6}$$

and the flux to the substrate is simply

$$F_B = F_A = A. \tag{A7}$$

In this limit, all ions diffuse to the substrate and the flux to the substrate is simply equal to the rate at which new ions are produced by beam ionization. The validity conditions for this limit are as follows: neglect of recombination in the source region requires

$$N_0 = A(B-A) + \tfrac{1}{2}A^2 << 1, \tag{A8a}$$

and evaluation of an iterative correction shows that the neglect of recombination in the transport region is valid if

$$A(B-A)^3 << 12. \tag{A8b}$$

Regime 2: Recombination dominant in the source (A large), but insignificant in the transport region (B–A small)

We consider next the limit where most of the ions produced in the source are lost to recombination, but little additional recombination occurs in the transport region. In the source region, we then expect N to be just less than its limiting value of unity, and we look for a solution to Eq. (A1a) in the form $N(X) \cong 1 - \delta N(X)$, linearizing in δN. We find the solution to be of the form

$$N(X) \cong 1 - (1-N_0)\cosh(\sqrt{2}X), \quad \text{for } X \le A. \tag{A9}$$

In the transport region we can use the solution (A5b). After matching at X = A, we find the central density N_0 to be

$$N_0 \cong 1 - \frac{1}{\sqrt{2}(B-A)\sinh(\sqrt{2}A) + \cosh(\sqrt{2}A)}, \tag{A10}$$

and the flux to the substrate to be

$$F_B \cong \frac{\sqrt{2}}{\sqrt{2}(B-A) + \coth(\sqrt{2}A)}. \tag{A11}$$

The validity conditions for this regime, in addition to A>>1 are

$$\sqrt{2}(B-A)\tanh(\sqrt{2}A) >> 1, \tag{A12a}$$

$$B - A << 3. \tag{A13b}$$

Regime 3: Recombination insignificant in the source (A small), but dominant in the transport region (B–A large)

In the source region, we again use Eq. (A5a) for N(X). In the transport region, we approximate the integral in Eq. (42b) by using the relation

$$\int_0^w \frac{d\tilde{w}}{\sqrt{1+\tilde{w}^3}} \cong \frac{2.86w}{2.5+w}, \tag{A14}$$

which gives

$$N(X) \cong \frac{0.87(B-X)F_B}{1 - 0.31(B-X)F_B^{1/3}}. \tag{A15}$$

Approximation (A14) is simple and yet is uniformly accurate to within 15% for any value of X.

In all cases, the flux F_B to the substrate is constrained to

$$F_B < \frac{35}{(B-A)^3}, \tag{A16}$$

to keep the denominator of Eq. (A15) positive. In the present limit, the substrate is remote from the source, and F_B is small because most of the ions recombine in the transport region before reaching the substrate. We shall show that (A16) must then become very nearly an equality, in order to prevent N_A from becoming vanishingly small.

Matching N(X) from (A5a) and (A15) at X = A we find

$$N(A) = N_0 - \tfrac{1}{2}A^2 = \frac{0.87\ (B-X)F_B}{1-0.31\ (B-X)F_B^{\,1/3}}, \tag{A17}$$

and matching the flux from (A4a) and (A5a) at X = A gives

$$F_A{}^2 = A^2 = F_B{}^2 + \tfrac{2}{3}\left(N_0 - \tfrac{1}{2}A^2\right)^3. \tag{A18}$$

Equation (A18) can be solved for the central density,

$$N_0 = \left(\tfrac{3}{2}\right)^{1/3} A^{2/3} + \tfrac{1}{2}A^2, \tag{A19}$$

and using (A18) in (A17) yields an equation for F_B,

$$1 - 0.31(B-A)F_B{}^{1/3} = \frac{0.87(B-A)F_B}{\left[\tfrac{3}{2}\left(A^2 - F_B{}^2\right)\right]^{1/3}}. \tag{A20}$$

When F_B is small, the RHS can be neglected, yielding the simple result alluded to previously,

$$F_B = \frac{35}{(B-A)^3}. \tag{A21}$$

This approximation is valid when the RHS of (A20) is << 1, which holds when

$$(B-A)A^{1/3} >> 5 \tag{A22}$$

In addition, the approximation in the source region requires $N_0 << 1$, and according to (56) this requires

$$A << 0.6. \tag{A23}$$

Regime 4: Recombination dominant in both the source and the transport region (A and B both large)

In this case both the source region and the transport region are thick, and ions are mostly lost to recombination in both regions. We use (A9) for N(X) in the source region, and (A15) in the transport region. The matching conditions for density and flux at X = A give, respectively

$$N_A = 1 - (1-N_0)\cosh(\sqrt{2}A) = \frac{0.87(B-A)F_B}{1-0.31(B-A)F_B{}^{1/3}}, \tag{A24}$$

$$F_A^2 = 2(1-N_0)^2 \sinh^2(\sqrt{2}A) = F_B^2 + \tfrac{2}{3}N_A^3. \tag{A25}$$

These equations yield an approximate solution

$$N_0 = 1 - \frac{1}{\sqrt{3}\sinh(\sqrt{2}A)}, \tag{A26}$$

$$F_B = \frac{35}{(B-A)^3}, \tag{A27}$$

valid when

$$A >> 1, \tag{A28}$$

$$B - A >> 8. \tag{A29}$$

The parameter space occupied by each of Cases 1 - 4 is shown in Fig. 4. There the boundaries of each region are drawn where equalities replace the strong inequality conditions.

Appendix B, Further Discussion of Two Dimensional Diffusion with Conducting Boundaries

For a strongly magnetized plasma with side walls biased strongly negative, our approximations are that the potential is given by Eq. (50), the density is a solution to Eq. (51), and the electron motion is only in the z direction. With these approximations, a simple Green's function solution gave the solution for density in Eq. (52). Now let us check the consistency of the solution. The electron continuity equation must also be satisfied, and our assumption has been that it is satisfied by electron flow in the z direction. Then the electron velocity is

$$u_{ez} = \frac{1}{n}\int_0^z S dz' \tag{B1}$$

where we have assumed that due to the symmetry about z = 0, $v_{ez}(z=0) = 0$. The correction term in the z component of the electron momentum equation is then

$$-\frac{mv_e}{n}\int_0^z S dz' \tag{B2}$$

and this must be small compared to the terms retained in this equation, e.g. $T\frac{\partial}{\partial z}\ln n$. Assuming the density drops from its maximum value to zero in a distance of L, we find that the assumption is verified as long as

$$mv_e SL << \frac{nT}{L} \tag{B3}$$

Assuming that the density is determined by Eq.(52), one can relate the central density to S and thereby derive the first inequality of Eq. (53a).

The collisions in the z component of the electron momentum equation effectively give a correction to ϕ of order

$$e\delta\phi = \int_0^z dz' \frac{mv_e}{n}\int_0^{z'} dz'' S \tag{B4}$$

Note that this correction to ϕ varies with x because n does. Our model assumes the $d\delta\phi/dx$ is small compared to the terms retained in the x component of the electron momentum equation. Also, this term leads to a z dependence of u_{ex} in the bulk plasma which cannot be canceled by simply varying the potential of the side wall. For our approximation to be valid, this velocity must be small compared to the ion velocity in the x direction. If we neglect the z dependence of S and n, we find that

$$e\delta\phi = \frac{m\nu_e S z^2}{2n(x)} \tag{B5}$$

so that the contribution of $d\delta\phi/dx$ to u_{ex} at z=L is given by

$$\delta u_{ex}(z = L) = \frac{\nu_e S L^2}{2\nu_e * n^2}\frac{\partial n}{\partial x} \tag{B6}$$

The ion velocity u_{ix} from the diffusion model is given roughly by D/b ~ Sb/n, so the condition $\delta u_{ex} << u_{ix}$ is

$$\frac{\nu_e{}^2 L^2}{2\Omega_e{}^2 b^2} << 1 \tag{B7}$$

This is the second inequality in Eq. (53b). It shows how large the magnetic field must be as a function of electron collisionality and system aspect ratio for cross field ambipolar diffusion to be suppressed in favor of electron flow along z. If Eqs. (B7 and B11) (and thereby Eq. (44)) are violated, electron motion cannot be one dimensional in z; u_{ex} will necessarily be non zero at points within the plasma bulk, even if it is zero on the wall itself. In that case, we expect that the density and flux will be non-uniform in z.

Acknowledgments The authors would like to thank Darren Leonhardt, Donald Murphy, and Scott Walton of NRL for a number of useful discussions. This work was supported by ONR.

References

[1] Asmussen J, 1989, J. Vac. Sci. Technol. A7, 883,1989

[2] Lampe M, Joyce G, Manheimer W M and Slinker S P, 1998, *IEEE. Trans. Plasma Sci.* 26, 1592-1609

[3] Hopwood J 1992 *Plasma Sources Sci. Technol.* **1**, 109-116

[4] Keller J H 1996 *Plasma Sources Sci. Technol* **5**, 166–172

[5] Boswell R W and Chen F F 1997 *IEEE Trans. Plasma Sci.* **25**, 1229–1244

[6] Chen F F and Boswell R W 1997 *IEEE Trans. Plasma Sci.* **25**, 1245–1257

[7] Manheimer W M 1991 *IEEE Trans. Plasma Sci.* **19**, 1228–1234

[8] Robson A E, Morgan R and Meger, R A 1992 *IEEE Trans. Plasma Sci.* **20**, 1036–1040

[9] Meger R A, Mathew J, Gregor J, Pechacek R, Fernsler R F, Manheimer W M and Robson A, *Phys. Plasmas* **2**, 2532–2538

[10] Mathew J, Fernsler R F, Meger R A, Gregor J, Murphy D, Pechacek R and Manheimer W M 1996 *Phys. Rev. Lett.* **77**, 1982–1985

[11] Fernsler R F, Manheimer W.M., Meger R A, Mathew J, Murphy D, Pechacek R and Gregor J 1998 *Phys. Plasmas* **5**, 2137–2144

[12] Murphy D, Fernsler R F, Pechacek R and Meger R A 1999 *IEEE Trans. Plasma Sci.* (to be published)

[13] Murphy D, Fernsler R F, Pechacek R and Meger R A 1999 *IEEE Trans. Plasma Sci.* (to be published)

[14] Manheimer W M, Fernsler R F and Gitlin M S, 1998, *IEEE Trans. Plasma Sci,* 26, 1543-1555

[15] Burdovitsin V, and E. Oks, 1999, Rev. Sci. Instruments, 70, 2975

[16] Murphy D, W. Amatucci, D. Leonhardt, S. Walton, R. Meger, and R. Fernsler, 1999 Bull. APS, vol. 44, no. 4, p. 58

[17] Walton S., D. Leonhardt, D. Murphy, R. Meger, and R. Fernsler, 1999 Bull. APS, vol. 44, no. 4, p. 58

[18] Jackson J D 1975 *Classical Electrodynamics* (New York: John Wiley and Sons), Chap. 13.

[19] L. Christophorou, 1971, *Atomic and Molecular Radiation Physics*, (John Wiley and sons, NY) p 36

[20] Ref. [18], using the expression for $d\theta^2/dz$ and relating it to momentum exchange cross section.

[21] Leonhardt D, S. Walton, D. Murphy, W. Amatucci, R. Meger, and R. Fernsler, 1999 Bull. APS, vol. 44, no. 4, p. 58

[22] S.C. Brown, *Basic Data of Plasma Physics, 1966*, p 199 MIT Press, Cambridge, MA, 1967

[23] Mul, P.M. and J.W. McGowan, 1979, *J. Phys. B*, 12, 1591-1601

[24] Itikawa, I., A. Ichimura, K. Onda, K. Sakimoto, and K. Takayanag, 1989, *J. Phys. Chem. Ref. Data*, 18, 23-42

[25] Lieberman M A and Lichtenberg A J 1994 *Principles of Plasma Discharges and Materials Processing* (New York: Wiley), p. 373–377

[26] Bobbio S M 1989 Review of Magnetron Etch Technology *SPIE Vol. 1185,* 262

[27] Lieberman M A and Lichtenberg A J 1994 *Principles of Plasma Discharges and Materials Processing* (New York: Wiley), Chapter 6.2

[28] Riemann K-U 1981 *Phys. Fluids* **24**, 2163–2172

[29] R. Hake and A. Phelps, Momentum Transfer Cross Sections for Electrons in O_2, CO, and CO_2, Phys. Rev., 158, 70-84, 1967

[30]The low energy value of σv for oxygen is inferred from H.W. Ellis, R.Y. Pai, and E.W. McDaniel, 1976, *Atomic Data and Nuclear Tables* 17, 177-210 for room temperature oxygen; the higher energy data is inferred from Brown [19], p 69

[31]B. Chapman, 1980, Glow Discharge Processing, Wiley and Sons, NY, p 84-91

[32] Lieberman M A and Lichtenberg A J 1994 *Principles of Plasma Discharges and Materials Processing* (New York: Wiley), chapter 14.3

[33] Meger R, R. Fernsler, M. Lampe, D. Leonhardt, W.M. Manheimer, D. Murphy, R. Pechacek, and S. Walton, 1999 Bull. APS, vol. 44, no. 4, p. 38

[34] Fernsler, R, W.M. Manheimer, M. Lampe, and R. Meger, 1999 Bull. APS, vol. 44, no. 4, p. 38

[35] Manheimer W, 2000, IEEE Trans. Plasma Sci. to be published, also see W. Manheimer, NRL Memo 99-8348, *Parameter Space for Collisionless RF Sheaths*, April, 1999

[36] Manheimer, W.M., M. Lampe and R. Fernsler, to be published

Figure Captions

1. A schematic of the LAPPS plasma processing system.
2. Demonstration of LAPPS etching of photoresist in an oxygen plasma.
3. The density profile and governing equations for the LAPPS plasma in the one dimensional diffusion approximation
4. The parameter space for the one dimensional diffusion model.
5. A schematic of the initial LAPPS ion collection experiment
6. Collector currents as a function of bias voltage. The light circles I_2 is for the plate 0.6 cm from the source edge, and the solid diamonds I_1 are for the plate 1 cm from the source edge.
7. Experimental results and theoretical calculation for the collector currents as a function of gas pressure for a bias voltage of minus 30 volts. The light circles I_2 are for the plate 0.6 cm for the source edge, and the solid diamonds I_1 are for the plate 1 cm away.

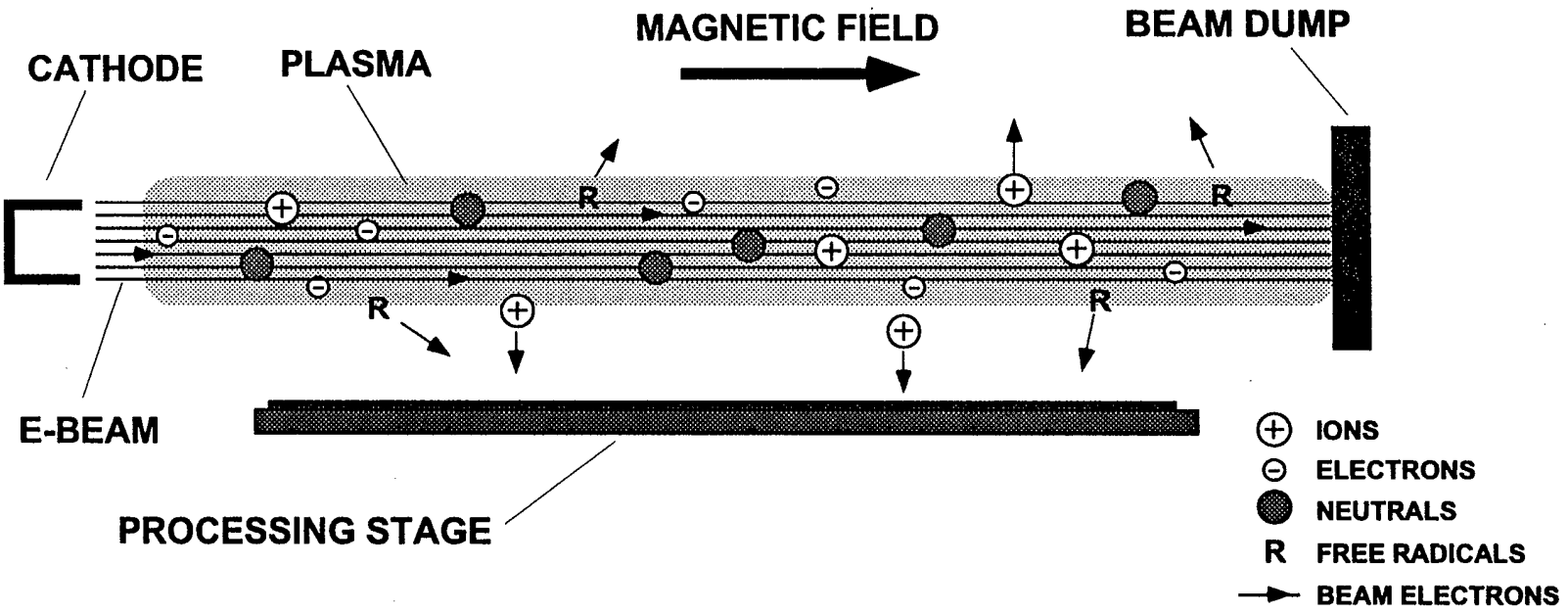
MAGNETIC FIELD
BEAM DUMP
CATHODE
PLASMA
R
R
R
R
E-BEAM
PROCESSING STAGE
IONS
ELECTRONS
NEUTRALS
R FREE RADICALS
BEAM ELECTRONS

Fig. 1

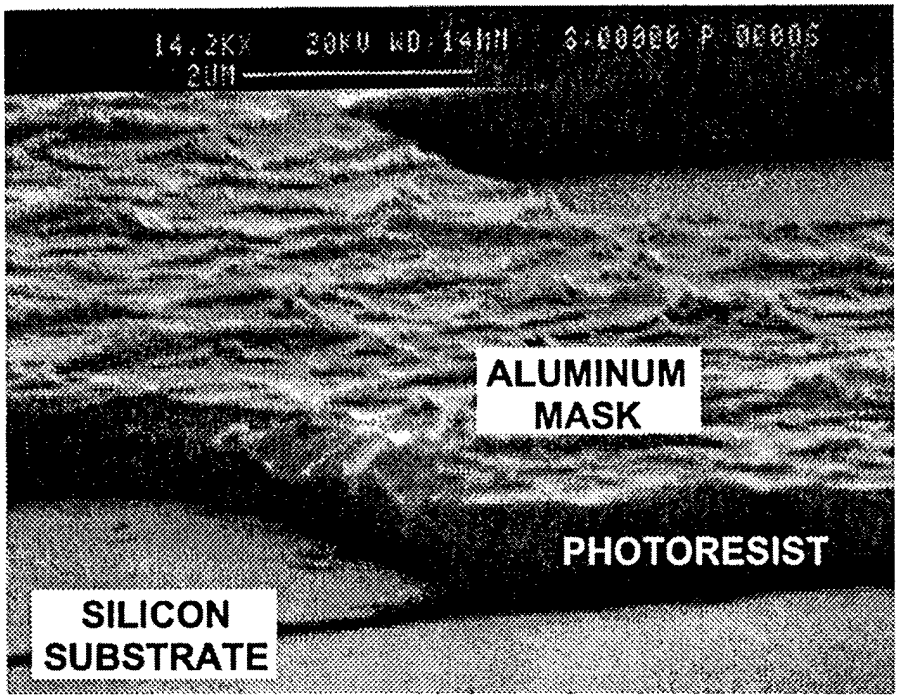
14.2KX 20KV WD:14MM
2UM
ALUMINUM MASK
PHOTORESIST
SILICON SUBSTRATE

Fig. 2

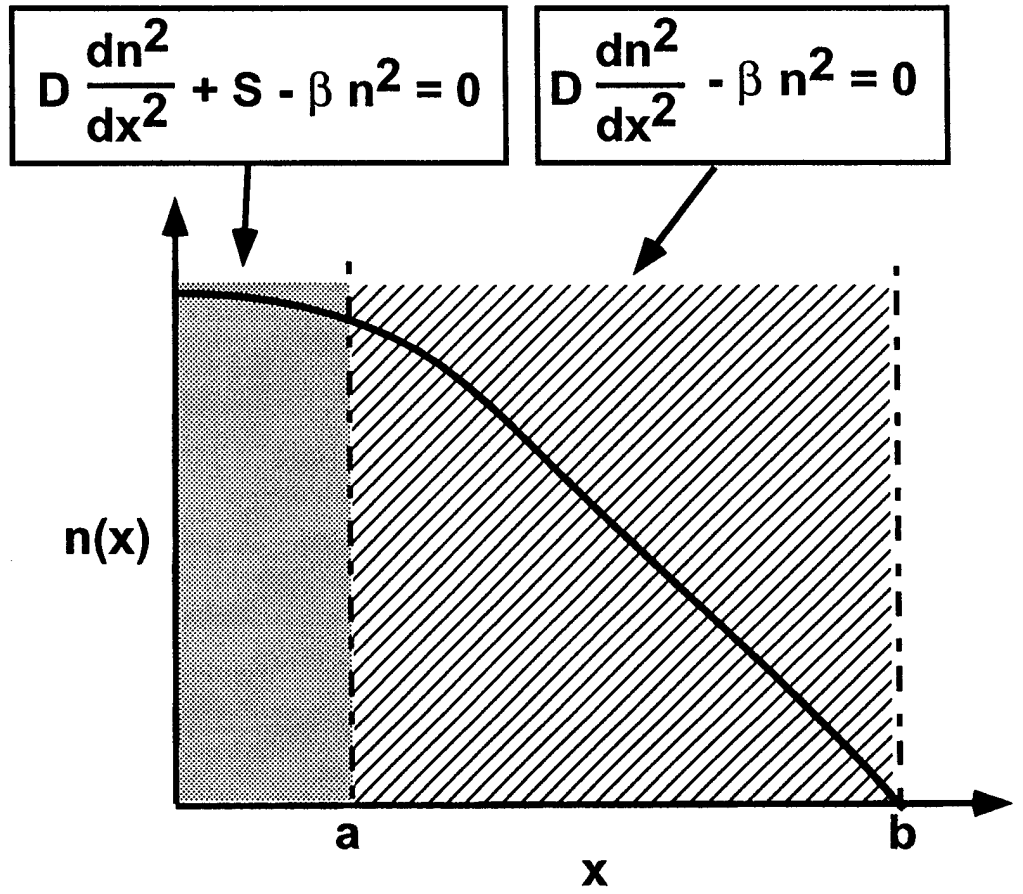

Fig. 3

40

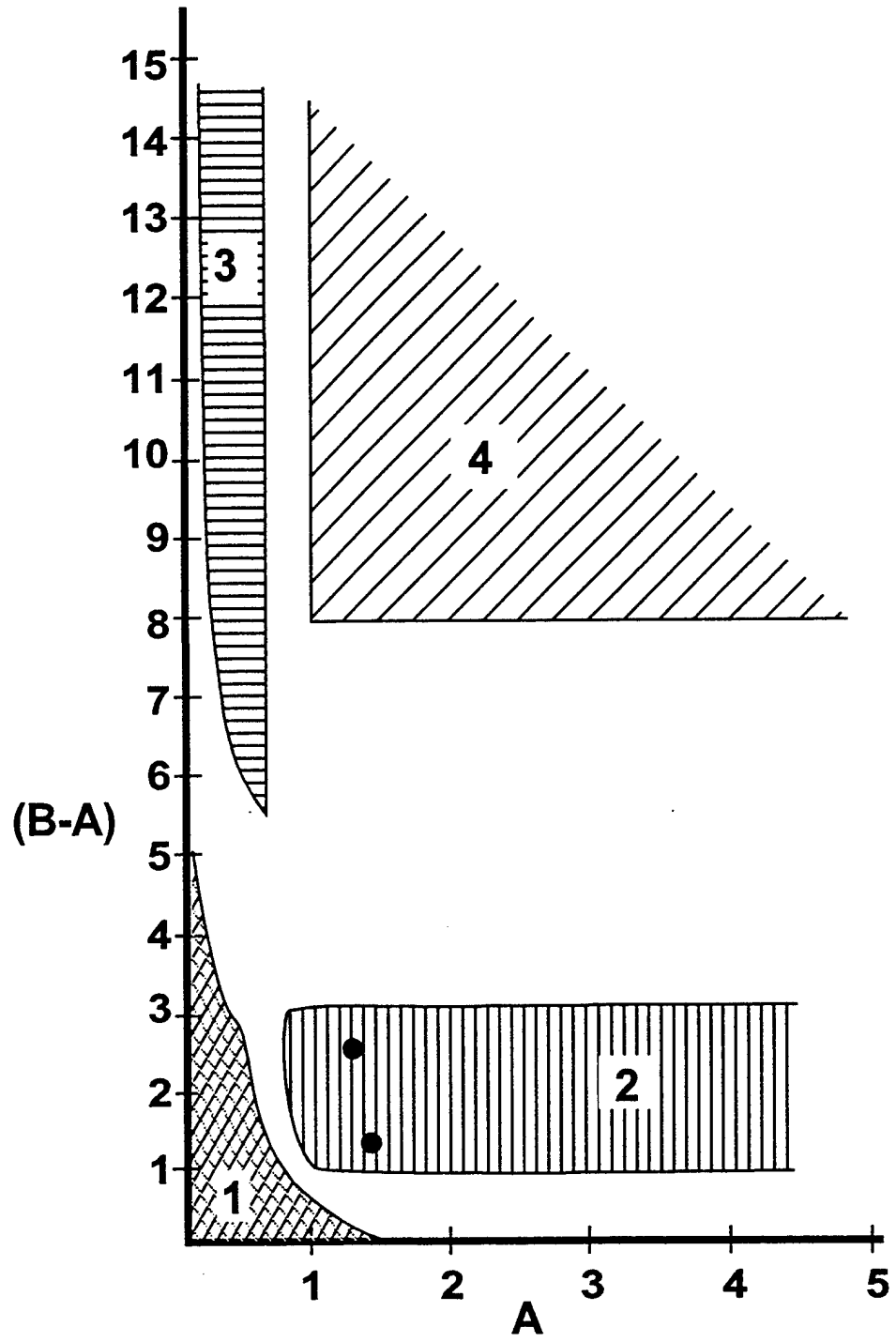

Fig. 4

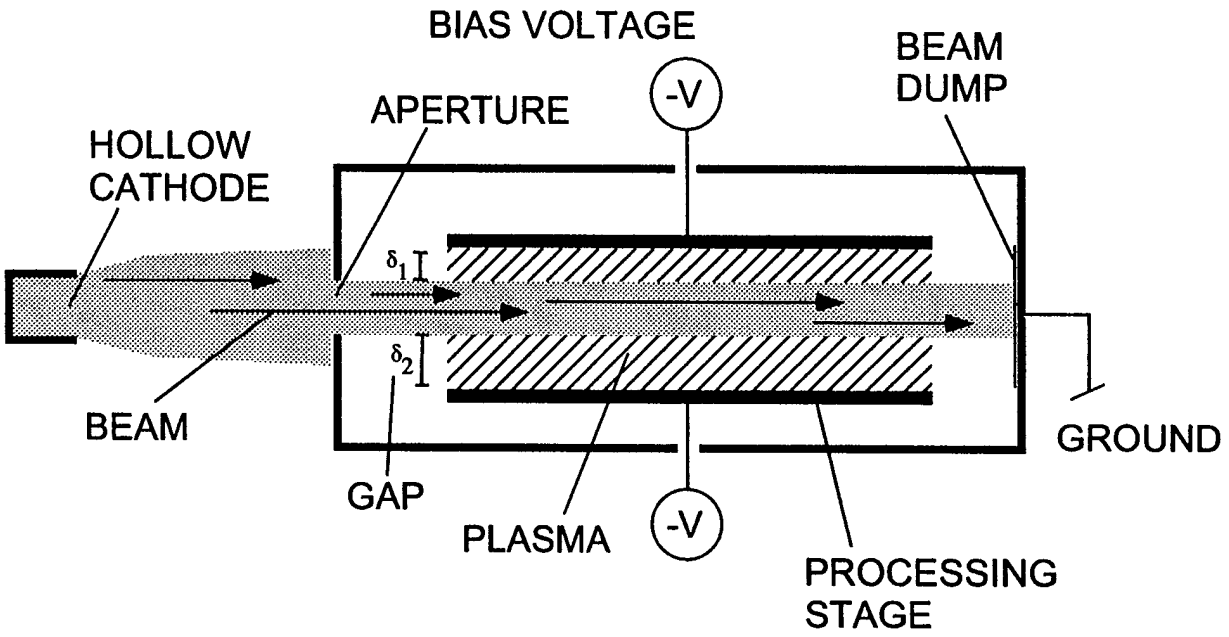
BIAS VOLTAGE
-V
BEAM
DUMP
APERTURE
HOLLOW
CATHODE
δ_1
δ_2
BEAM
GAP
PLASMA
-V
GROUND
PROCESSING
STAGE

Fig. 3

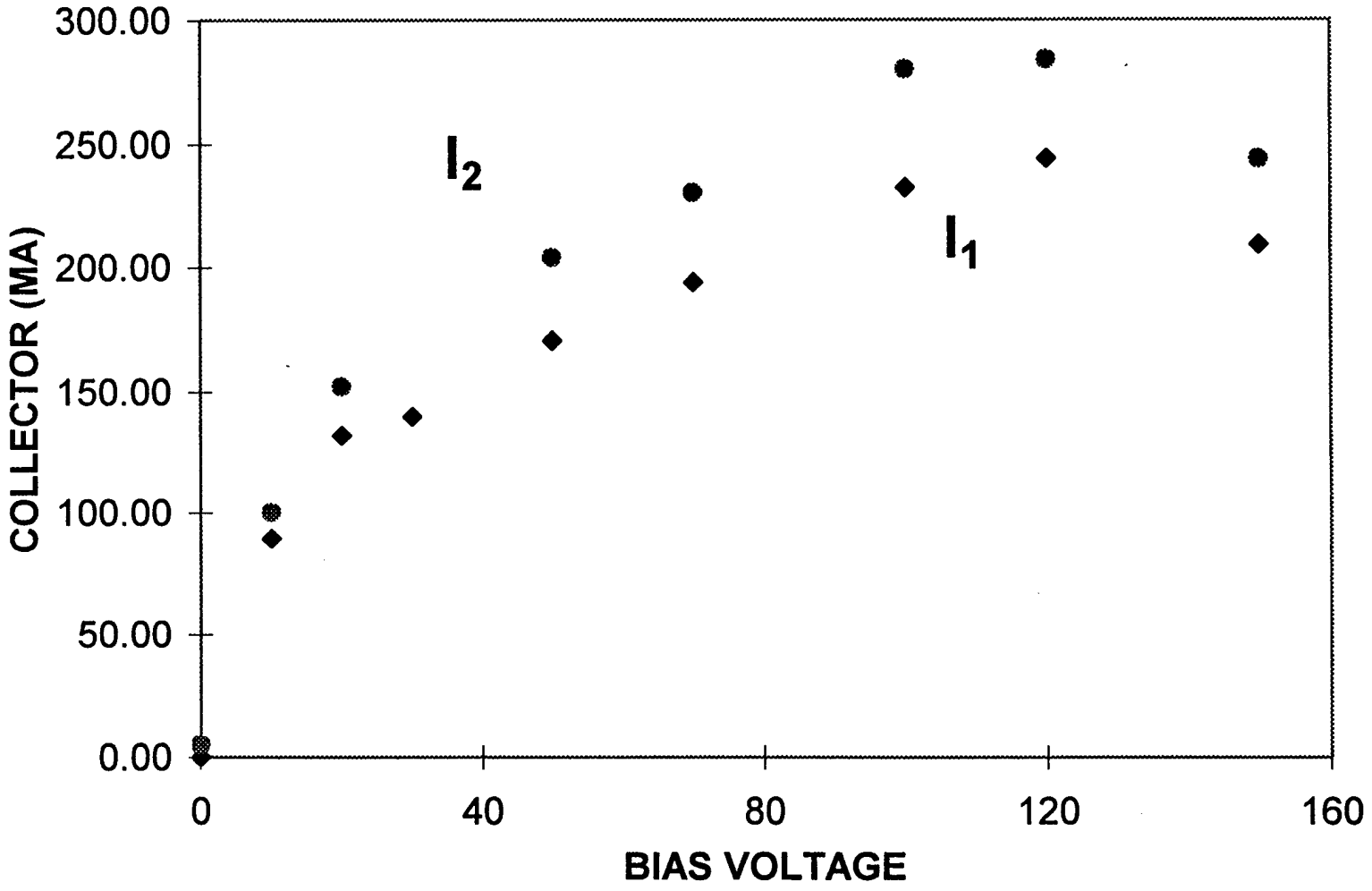
300.00
250.00
200.00
150.00
100.00
50.00
0.00
COLLECTOR (MA)
0
40
80
120
160
BIAS VOLTAGE
I2
I1

Fig. 6

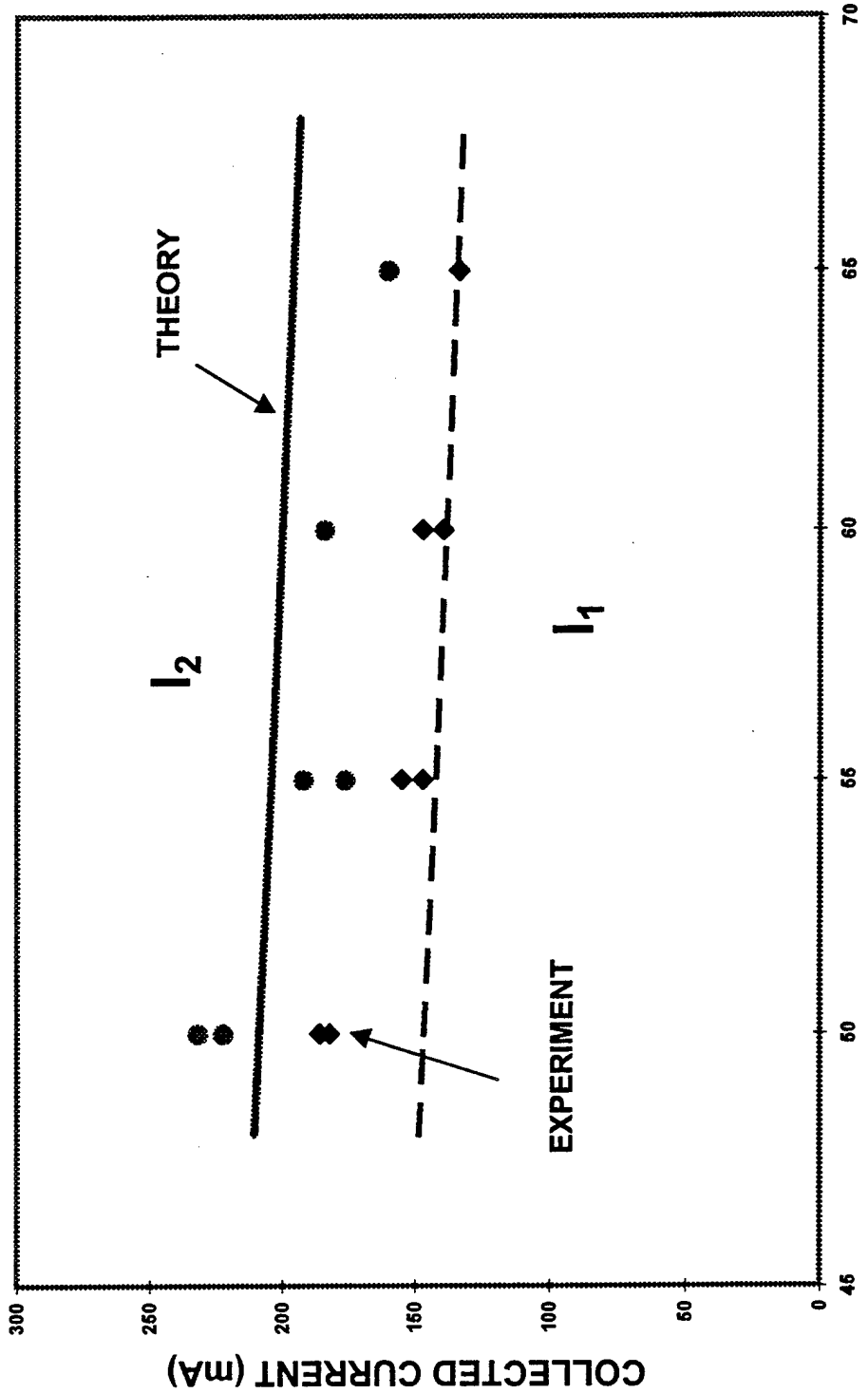
COLLECTED CURRENT (mA)
300
250
200
150
100
50
0
45
50
55
60
65
70
P (mT O2)
THEORY
I2
I1
EXPERIMENT

Fig. 7